

# Pion production in nucleon-nucleon collisions in chiral effective field theory with Delta(1232)-degrees of freedom.

A. A. Filin and V. Baru

*Institut für Theoretische Physik II,  
Ruhr-Universität Bochum, D-44780 Bochum, Germany and*

*Institute for Theoretical and Experimental Physics,  
117218, B. Cheremushkinskaya 25, Moscow, Russia*

E. Epelbaum and H. Krebs

*Institut für Theoretische Physik II,  
Ruhr-Universität Bochum, D-44780 Bochum, Germany*

C. Hanhart

*Institut für Kernphysik, (Theorie) and Jülich Center for Hadron Physics,  
Forschungszentrum Jülich, D-52425 Jülich, Germany and  
Institute for Advanced Simulation, Forschungszentrum Jülich, D-52425 Jülich, Germany*

F. Myhrer

*Department of Physics and Astronomy,  
University of South Carolina, Columbia, SC 29208, USA*

## Abstract

A calculation of the pion-production operator up to next-to-next-to-leading order for s-wave pions is performed within chiral effective field theory. In the previous study [Phys. Rev. C 85, 054001 (2012)] we discussed the contribution of the pion-nucleon loops at the same order. Here we extend that study to include explicit Delta degrees of freedom and the  $1/m_N^2$  corrections to the pion-production amplitude. Using the power counting scheme where the Delta-nucleon mass difference is of the order of the characteristic momentum scale in the production process, we calculate all tree-level and loop diagrams involving Delta up to next-to-next-to-leading order. The long-range part of the Delta loop contributions is found to be of similar size to that from the pion-nucleon loops which supports the counting scheme. The net effect of pion-nucleon and Delta loops is expected to play a crucial role in understanding of the neutral pion production data.

## I. INTRODUCTION

The reaction  $NN \rightarrow NN\pi$ , being the first inelastic channel of  $NN$  interaction, provides a good possibility to study  $NN$  dynamics at intermediate energies. The interest in pion production in  $NN$  collisions was revived almost 20 years ago when it was proposed [1, 2], that the process may be studied in a model-independent way within chiral perturbation theory (ChPT) — the low-energy effective field theory of QCD — lately reviewed in Refs. [3, 4]. In this effective field theory the approximate chiral symmetry of QCD is exploited in a systematic way. The study of the  $NN \rightarrow NN\pi$  reaction at threshold builds on the detailed understanding of the necessary two-body ingredients, the  $\pi N$  and  $NN$  interactions and reactions, which have been successfully evaluated within ChPT at low energies, see, e.g., Refs. [5] and [6] for recent reviews.

Surprisingly, the naive application of the standard ChPT power counting, where one assumes the typical momenta  $|\vec{p}|$  to be of the order of the pion mass  $m_\pi$ , to the reaction  $NN \rightarrow NN\pi$  by Refs. [2, 7–11], did not only fail to describe the data, especially in the  $pp \rightarrow pp\pi^0$  channel, but also revealed a problem with the convergence of the chiral expansion. However, in Ref. [1, 12] it was advocated that the proper treatment of the reaction  $NN \rightarrow NN\pi$  requires taking into account the new intermediate momentum scale,  $p = |\vec{p}| \sim \sqrt{m_\pi m_N}$  ( $m_N$  is the nucleon mass), which corresponds to the relative momentum of the initial nucleons required to produce a pion at threshold. This new scale led to a new hierarchy of diagrams driven by the expansion parameter

$$\chi_{\text{MCS}} \simeq \frac{m_\pi}{p} \simeq \frac{p}{\Lambda_\chi} \simeq \sqrt{\frac{m_\pi}{m_N}}, \quad (1)$$

with  $\Lambda_\chi \simeq m_N$  being the typical hadronic scale. In what follows, we will refer to this power counting as the momentum counting scheme (MCS). The MCS has been applied in a variety of pion threshold production reactions for the outgoing pion in an s-wave [13–18] and p-wave [19–21], and for isospin violating pion production reactions [22–24].

It has been known for years that the strength of the s-wave pion production amplitude in the charged channels  $pp \rightarrow d\pi^+$  and  $pp \rightarrow pn\pi^+$  is dominated by the leading order (LO) Weinberg–Tomozawa (WT) operator [25]. On a more quantitative level, the cross sections for these two reactions were underestimated by a factor of 2 [3]. Meanwhile, the application of the MCS to s-wave production in the  $pp \rightarrow d\pi^+$  channel at next-to-leading order (NLO) [14], revealed quite good agreement with experimental data. To obtain this agreement it was important to realize that the nucleon recoil corrections  $\propto 1/m_N$  contribute in MCS at lower order than what is indicated naively by the order of the Lagrangian since in MCS  $p^2/m_N \sim m_\pi$ . In effect, the leading WT operator was enhanced by a factor 4/3 due to the recoil correction to the WT pion rescattering vertex. This enhancement resulted in an increase of the cross section by about the missing factor 2. In contrast, for s-wave pion production in the neutral channel  $pp \rightarrow pp\pi^0$ , the situation is completely different. In this channel the large isovector WT rescattering vertex does not contribute while the direct emission of the pion from one-nucleon leg at LO is dynamically strongly suppressed [1]. Furthermore, the resulting contribution of loops at NLO was shown to vanish both for the  $pp \rightarrow pp\pi^0$  [13] and  $pp \rightarrow d\pi^+$  [14] reaction channels. In fact, we believe that the experimentally measured  $pp \rightarrow pp\pi^0$  reaction is unique in that it directly probes the higher order MCS contributions which in the charged channels are masked by the dominant lower order Weinberg–Tomozawa term. Following this logic, in Ref. [16] we extended the analysis

of pion-nucleon loops to next-to-next-to-leading order (N<sup>2</sup>LO). The pertinent results of Ref. [16] can be summarized as follows:

- significant cancellations of loops found at NLO are also operative at N<sup>2</sup>LO. In particular, all loop topologies involving  $1/m_N$  corrections to the leading vertices cancel completely, as do the loops involving low-energy constants (LECs)  $c_i$ .
- the cancellation of pion-nucleon loops at N<sup>2</sup>LO is not complete yielding a non-vanishing N<sup>2</sup>LO contribution.
- using dimensional regularization, all UV divergencies in the loops were absorbed into redefinition of low-energy-constants (LECs) in the Lagrangian at N<sup>2</sup>LO. These LECs parametrize short-range physics not resolved explicitly at the energies relevant for pion production at threshold.
- the scheme-independent long-range part of pion-nucleon loops was found to be of a natural size as expected from the MCS, both for charged and neutral pion production. This puts in question the earlier phenomenological studies [26–32] of these reactions where none of these N<sup>2</sup>LO loop contributions were considered.

Due to the fact that the Delta-nucleon ( $\Delta$ -N) mass splitting,  $\delta = m_\Delta - m_N$ , is numerically of the order of  $p$  (i.e.  $\delta \sim p$ ), the Delta-isobar should be explicitly included as a dynamical degree of freedom<sup>1</sup> [1, 12, 13]. At tree-level, the effect of the Delta manifests itself already at NLO as discussed within chiral EFT in Refs. [1, 12, 13, 34]. In addition, starting from NLO the Delta-resonance also gives rise to loop contributions which at NLO were shown in Ref. [13] to cancel exactly both for the neutral and charged channels. Meanwhile, the role of the Delta loops at N<sup>2</sup>LO has not been discussed in the literature and is a topic of the present investigation.

In this work we complete the calculation of the loop diagrams for the s-wave pion-production operator at N<sup>2</sup>LO. In particular, the previous calculation [16] is extended and improved in the following aspects:

- we treat the Delta-resonance as an explicit virtual degree of freedom in all loops and confirm the cancellation of all loop contributions containing Delta at NLO.
- we extend the calculation of the loops with the explicit Delta to N<sup>2</sup>LO. It is found that some of the loops renormalize the bare  $\pi NN$  coupling constant while a group of other N<sup>2</sup>LO loop diagrams vanishes in a close analogy with pion-nucleon loops.
- the N<sup>2</sup>LO remnant of the loops yields a long-range contribution to the pion-production operator amplitudes similar in size to those from pion-nucleon loops at the same order.
- we include the  $1/m_N^2$  corrections to the tree-level operators at N<sup>2</sup>LO and present the operator for s-wave pion production with explicit Delta degrees of freedom up-to-and-including N<sup>2</sup>LO.

---

<sup>1</sup> In Ref.[33] the same power counting was applied to study Compton scattering off the nucleon in the delta region

The paper is organized as follows. In the next section we review the arguments and results of Ref. [16]. In particular, in this section we present some features special to the MCS. In Sec. II we discuss the cancellation mechanism of NLO loop diagrams before we explicitly give the expressions for the tree-level and loop-diagram production operators to N<sup>2</sup>LO derived in Ref. [16]. In Sec. III we present the Lagrangian which includes the  $\Delta$ , give the tree-level amplitudes for the  $\Delta$  contribution to s-wave pion production and then evaluate all the loop diagrams involving Delta excitation to N<sup>2</sup>LO. Here we heavily rely on the arguments presented in Sec. II. The last subsection in Sec. III contains the details on regularization of the UV divergences present in the loop diagrams including a discussion of the necessary decoupling requirements in the heavy  $\Delta$  mass limit. In Sec. IV we compare the pion-nucleon and  $\Delta$ -loop contributions before we make our conclusions in the last section.

## II. S-WAVE PION PRODUCTION TO N<sup>2</sup>LO: THE CONTRIBUTIONS OF PION AND NUCLEON DEGREES OF FREEDOM

For completeness and to prepare the stage for the main part of the paper, where the inclusion of the  $\Delta$  as dynamical degree of freedom is discussed, in this section we summarize the results of Ref. [16].

### A. Diagrams and Power Counting

The most general form of the threshold amplitude (where the pion is in an s-wave relative to a  $NN$  S-wave final state) for the pion-production reaction  $N_1(\vec{p}) + N_2(-\vec{p}) \rightarrow N + N + \pi$  in the center-of-mass frame can be written as [16]:

$$M_{th}(NN \rightarrow NN\pi) = \mathcal{A}(\vec{\sigma}_1 \times \vec{\sigma}_2) \cdot \vec{p} \, \tau_+ \cdot \phi^* + \mathcal{B}(\vec{\sigma}_1 + \vec{\sigma}_2) \cdot \vec{p} \, (-i) \tau_x \cdot \phi^*, \quad (2)$$

where  $\tau_+ = \tau_1 + \tau_2$ ,  $\tau_x = i \tau_1 \times \tau_2$  and  $\vec{\sigma}_{1,2}$  and  $\tau_{1,2}$  are the spin and isospin operators of nucleons 1 and 2. This expression incorporates the selection rules for the  $NN$  states. The final pion's isospin state is denoted by  $\phi$ , e.g.  $\phi = (0, 0, 1)$  for  $\pi^0$ -production and  $\phi = (1, i, 0)/\sqrt{2}$  for  $\pi^+$ -production. For example, the amplitude  $\mathcal{A}$  corresponds to the production of an s-wave pion accompanied with the final state spin-singlet S-wave  $NN$  interaction ( $pp \rightarrow pp\pi^0$ ), while  $\mathcal{B}$  corresponds to the spin triplet  $NN$  final state ( $pp \rightarrow d\pi^+$ ).

As mentioned in the introduction, the reaction  $NN \rightarrow NN\pi$  at threshold involves momenta of ‘‘intermediate range’’  $p \approx \sqrt{m_\pi m_N}$ , Eq. (1). For near threshold s-wave pion production, the outgoing two-nucleon pair has a low relative three-momentum  $p'$  and appears therefore predominantly in S-wave. We therefore assign  $p'$  an order  $m_\pi$ , i.e, the expansion parameter in Eq. (1) is augmented by  $\chi_{MCS} \simeq p'/p \simeq m_\pi/p \simeq p/m_N$ .

The calculations are based on the effective chiral Lagrangian given explicitly in Ref. [16], see Refs. [35–38] for more details. To N<sup>2</sup>LO, one needs to keep the corrections  $\sim 1/m_N^2$ , as will be shown below. This means that we need to keep vertices  $\sim 1/m_N^2$  from the pion-nucleon Lagrangian  $\mathcal{L}_{\pi N}^{(3)}$  [37, 38]. In Appendix B the terms in the Lagrangian relevant for our study are listed explicitly.

The diagrams containing only pion and nucleon degrees of freedom that contribute to the reaction  $NN \rightarrow NN\pi$  up to N<sup>2</sup>LO in the MCS expansion, are shown in Fig. 1. The first row of diagrams represents contributions at LO. In the first row the first two diagrams are

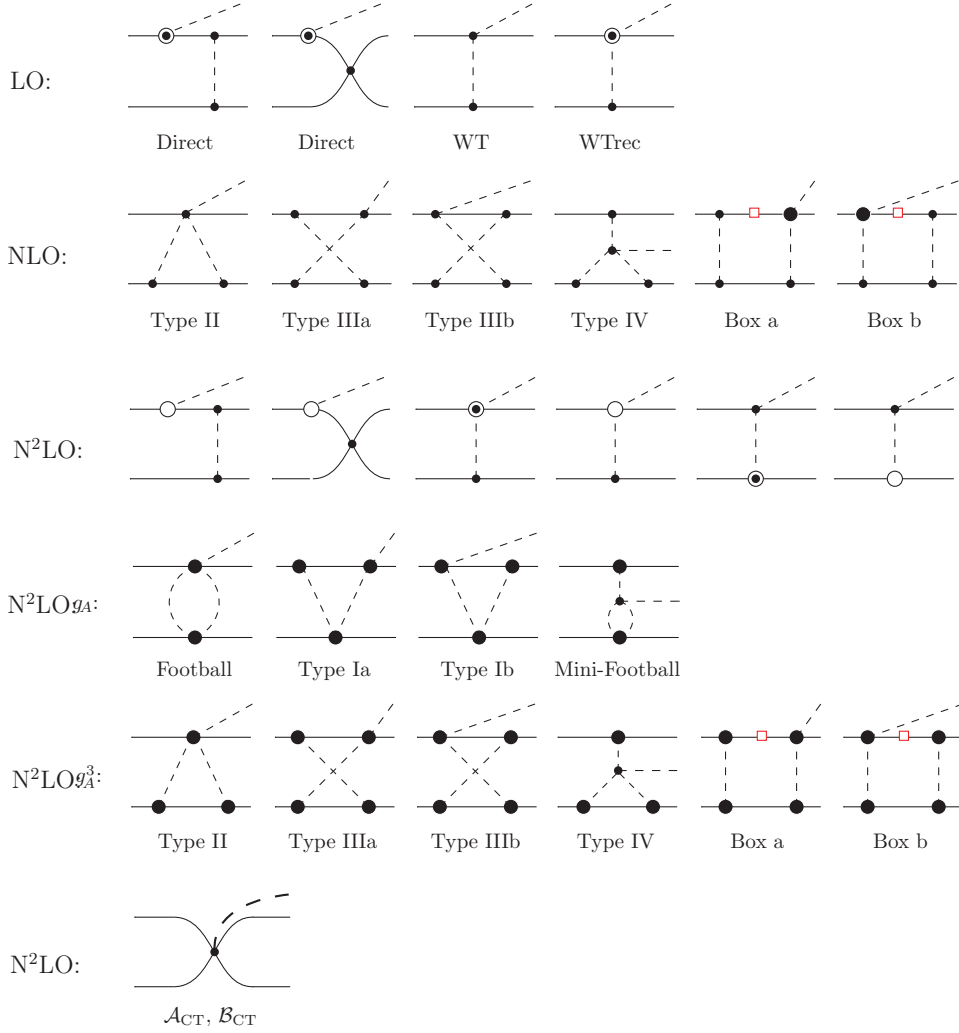


FIG. 1: Complete set of diagrams up to  $N^2\text{LO}$  (in the  $\Delta$ -less theory) for s-wave pions. Solid (dashed) lines denote nucleons (pions). Solid dots correspond to the leading vertices from  $\mathcal{L}_{\pi N}^{(1)}$  and  $\mathcal{L}_{\pi\pi}^{(2)}$ ,  $\odot$  stands for the sub-leading vertices from  $\mathcal{L}_{\pi N}^{(2)}$  whereas the blob indicates the possibility to have both leading and subleading vertices from  $\mathcal{L}_{\pi N}^{(1)}$  and  $\mathcal{L}_{\pi N}^{(2)}$  (see Fig. 2 for an illustration), the opaque symbol  $\circ$  stands for the vertices  $\sim 1/m_N^2$  from  $\mathcal{L}_{\pi N}^{(3)}$ . The  $NN$  contact interaction in the top row is represented by the leading S-wave LECs  $C_S$  and  $C_T$  from  $\mathcal{L}_{NN}$  whereas the contact five-point vertices in the bottom row are given by the LECs  $\mathcal{A}_{CT}$  and  $\mathcal{B}_{CT}$ . The red square in the box diagrams indicates that the corresponding nucleon propagator cancels with parts of the  $\pi N$  vertex and leads to the irreducible contribution, see text for further details.

sometimes called the “direct” one-nucleon diagrams or impulse-approximation diagrams in the literature, whereas the other two graphs are called rescattering diagrams. At NLO for s-wave pion production loop diagrams start to contribute, as shown by the second row of graphs. As will be reviewed below, these NLO amplitudes cancel completely [13–16]. At  $N^2\text{LO}$ , there are several contributing tree-level diagrams which are topologically similar to those at LO but with sub-leading vertices from  $\mathcal{L}_{\pi N}^{(2)}$  and even  $\mathcal{L}_{\pi N}^{(3)}$ . These diagrams are shown in the third row in Fig. 1. In addition, one needs to account for the pion-nucleon

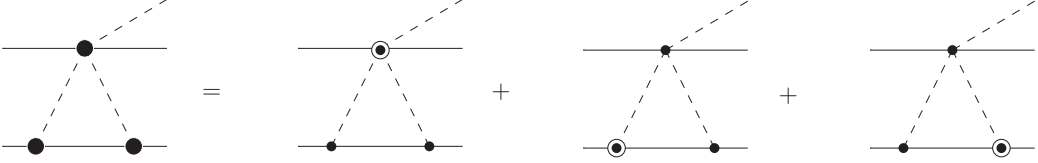


FIG. 2: An example illustrating the notation used for N<sup>2</sup>LO operators in Fig.1. The sub-leading vertex should only appear at one vertex in each diagram.

loops which, at this order, can be combined in two series of amplitudes, one proportional to  $g_A^3$  with a topology like the NLO pion-nucleon loop diagrams and one proportional to  $g_A$ . These diagrams are given in rows four and five in Fig. 1, respectively. To the order we are working, it suffices to include the sub-leading vertex from  $\mathcal{L}_{\pi N}^{(2)}$  only once (but we have to consider all permutations of  $\mathcal{L}_{\pi N}^{(2)}$  acting on a vertex) in the loops while retaining the other vertices at leading order as illustrated in Fig.2.

For illustration of how the order of diagrams are estimated (or counted) in the MCS, we concentrate on the tree-level rescattering diagrams in Fig. 1 and will compare the LO and the sub-leading diagrams designated as N<sup>2</sup>LO in Fig. 1. First we consider the rescattering diagram in the first and third row where the  $\pi NN$  vertex on the lower nucleon line originates from  $\mathcal{L}_{\pi N}^{(1)}$ . In Eq. (3) below, the  $p/f_\pi$  and  $1/p^2$  in front of the curly bracket stand for the dimensional estimate of the  $\pi NN$  vertex and the pion propagator, whereas the expressions after the curly bracket multiplied by  $1/f_\pi^2$  originate from the rescattering vertices and correspond to the  $\pi N$  scattering vertices from  $\mathcal{L}_{\pi N}^{(1)}$  and  $\mathcal{L}_{\pi N}^{(2)}$  [first row in Eq. (3)],  $\mathcal{L}_{\pi N}^{(2)}$  [second row in Eq. (3)] and  $\mathcal{L}_{\pi N}^{(3)}$  [third row]:

$$M_{\text{rescat}} \propto \frac{p}{f_\pi} \frac{1}{p^2} \frac{1}{f_\pi^2} \left\{ \begin{array}{l} m_\pi; \quad \left( \text{or } \frac{p^2}{m_N} \right) \\ \frac{m_\pi}{m_N} p; \quad \left( \text{or } m_\pi p c_i \right) \\ \frac{p^3}{m_N^2}; \quad \left( \text{or } \frac{p^3 c_i}{m_N} \right), \end{array} \right. = \frac{\chi_{\text{MCS}}}{f_\pi^3} \left\{ \begin{array}{ll} 1 & \text{--- LO} \\ \chi_{\text{MCS}}^2 & \text{--- N}^2\text{LO} \\ \chi_{\text{MCS}}^2, & \text{--- N}^2\text{LO}, \end{array} \right. \quad (3)$$

The LO operator scales as  $\sim \chi_{\text{MCS}}/f_\pi^3$  for s-wave pions. As seen in the last two rows of terms in Eq.(3) both the  $1/m_N$  corrections from  $\mathcal{L}_{\pi N}^{(2)}$  and the  $1/m_N^2$  corrections from  $\mathcal{L}_{\pi N}^{(3)}$  need to be taken into account at N<sup>2</sup>LO. Meanwhile, the inclusion of a  $1/m_N^2$  correction in the loops results in a higher-order diagram and is ignored. Analogously, the estimated order of the “direct” and rescattering contributions with sub-leading  $\pi NN$  vertices from  $\mathcal{L}_{\pi N}^{(2)}$  and  $\mathcal{L}_{\pi N}^{(3)}$  yield the same results. For example, for the “direct” contribution one finds  $[pm_\pi^2/(f_\pi m_N^2)][1/m_\pi][1/f_\pi^2] = \chi_{\text{MCS}}^3/f_\pi^3$ , which generates an amplitude at N<sup>2</sup>LO. To obtain this we used that the first term on the l.h.s corresponds to the  $\pi NN$  vertex from  $\mathcal{L}_{\pi N}^{(3)}$ , the next term reflects the energy  $v \cdot p \sim m_\pi$  of the nucleon propagator while the last term corresponds to the estimate of the one-pion exchange (OPE) or the contact term. Notice that while the tree-level contributions at N<sup>2</sup>LO with the sub-leading vertices from  $\mathcal{L}_{\pi N}^{(2)}$  were already taken into account in the literature, see e.g. Refs. [1, 12], the corrections stemming from  $\mathcal{L}_{\pi N}^{(3)}$  are new and derived here for the first time.

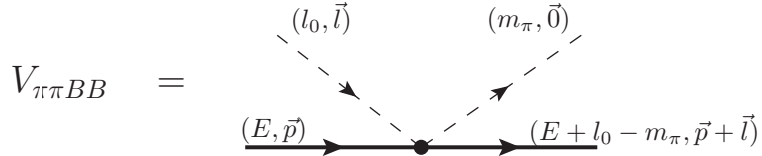


FIG. 3: The pion-baryon ( $\pi B \rightarrow \pi B$ ) transition vertex: definition of kinematical variables as used in Eq. (4). Solid thick lines stand for the baryon (nucleon or  $\Delta$ ) fields, dashed lines denote pions.

Before discussing the results at N<sup>2</sup>LO, one comment is in order. We noticed above that the loop diagrams at NLO cancel exactly. Here we want to explain the cancellation pattern in more detail since it is quite general and will be used later to establish cancellations among the loops at N<sup>2</sup>LO both with nucleons and Delta.

For the channel  $pp \rightarrow pp\pi^0$ , the sum of NLO diagrams of type II, III and IV in Fig. 1 is zero due to a cancellation between individual diagrams [13], while the box diagrams vanish due to the isovector nature of the WT operator. However, the same diagrams II–IV give a finite contribution to the channel  $pp \rightarrow d\pi^+$  [13]. As a result, the net contribution of these diagrams depends linearly on the  $NN$  relative momentum which implies a large sensitivity to the short-distance  $NN$  wave functions [39]. This seeming puzzle was solved in Ref. [14], where it was demonstrated that for the deuteron channel there is an additional contribution at NLO, namely the box diagrams in Fig. 1, stemming from the time-dependence of the WT pion-nucleon vertex. To demonstrate this, we write the expression for the Weinberg–Tomozawa pion-baryon (nucleon or  $\Delta$ ) scattering vertex in the notation of Fig. 3 as:

$$\begin{aligned}
 V_{\pi\pi BB} &= l_0 + m_\pi - \frac{\vec{l} \cdot (2\vec{p} + \vec{l})}{2m_B} \\
 &= 2m_\pi + \left( l_0 - m_\pi + E - \frac{(\vec{l} + \vec{p})^2}{2m_B} - \delta + i0 \right) - \left( E - \frac{\vec{p}^2}{2m_B} - \delta + i0 \right), \quad (4)
 \end{aligned}$$

where we kept the leading WT vertex and its baryon recoil correction, which are of the same order in the MCS, as explained above. If the baryon line is a nucleon one has  $\delta = 0$ , whereas  $\delta \neq 0$  for the case of the  $\Delta$ . For simplicity, we omit the isospin dependence of the vertex. The first term in the last line is the WT-vertex for kinematics corresponding to the on-shell incoming and outgoing baryons, the second term is the inverse of the outgoing baryon propagator while the third one is the inverse of the incoming baryon propagator. Note that for on-shell incoming and outgoing baryons, the expressions in brackets in (4) vanish, and the  $\pi$  baryon scattering vertex takes its on-shell value  $2m_\pi$  (even if the incoming pion is off-shell). A second consequence of Eq. (4) is that only the first term leads to a reducible diagram when the rescattering diagram with the  $\pi B \rightarrow \pi B$  vertex is convoluted with  $NN$  wave functions. The second and third terms in Eq. (4), however, lead to irreducible contributions, since one of the baryon propagators gets cancelled. This cancellation is illustrated by red squares on the nucleon propagators in the two box diagrams of Fig. 1. It was shown explicitly in Ref. [14] that those induced irreducible contributions cancel exactly the finite remainder of the NLO loops (II–IV) in the  $pp \rightarrow d\pi^+$  channel. As a consequence, there are no contributions at NLO for both  $\pi^0$  and  $\pi^+$  productions, see also our results in the two first rows of Tables I and II of Ref. [16].

In Ref. [16] we extended the analysis of the previous studies and evaluated the contribution from pion-nucleon loops at N<sup>2</sup>LO. As follows from Eq.(4), the part of the  $\pi N$  vertex in the diagrams IIIa, IIIb and Box a, Box b (the operators  $\propto g_A^3$ ) and Ia and Ib (the operators  $\propto g_A$ ) cancels the nucleon propagator yielding the contribution that has a topology of the diagrams II or “football”, respectively. Interestingly, the diagrams IV and “mini-football” also acquire contributions topologically similar to the diagrams II and “football” after canceling one of the pion propagators by a part of the four-pion vertex. In conclusion, Ref. [16] found that only those parts of the  $g_A^3$  ( $g_A$ )-diagrams which cannot be reduced to the topology of the diagram II (football) in Fig. 1, give a non-zero contribution to the transition amplitude. Thus, only very few N<sup>2</sup>LO contributions to the pion-production amplitude remain. Especially, all recoil corrections  $\propto 1/m_N$  and also all corrections  $\propto c_i$  vanish completely in the sum of the loop diagrams at N<sup>2</sup>LO. The non-vanishing amplitudes emerge from the diagrams IIIa, IIIb and IV in the case of the  $g_A^3$ -graphs and from the diagrams Ia, Ib and “mini-football” for the  $g_A$ -operators, where all the vertices, except for the recoil correction to the WT vertex, originate from the leading Lagrangian  $\mathcal{L}_{\pi N}^{(1)}$ . The explicit expressions of the resulting amplitudes are given in Sec.II C.

## B. Pion-production operator from tree-level diagrams

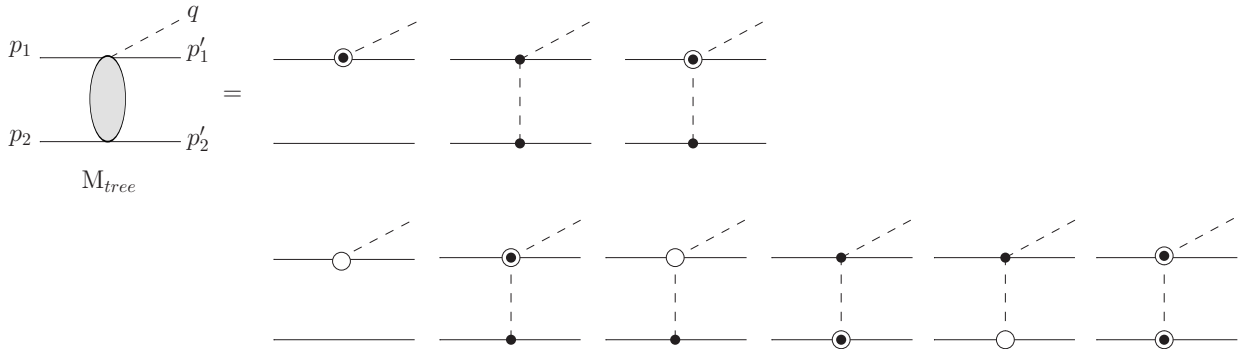


FIG. 4: Single-nucleon and rescattering diagram contributions to s-wave pion production up to N<sup>2</sup>LO: the diagrams in the first row on the r.h.s appear at LO, the diagrams in the second row give the N<sup>2</sup>LO contributions. The last diagrams in the first and second rows involve the WT recoil correction, whereas the second diagram in the second row involves the  $c_i$  rescattering vertex.

In this section we derive the amplitudes from diagrams shown in Fig. 4 up-to-and-including N<sup>2</sup>LO in the theory involving pion and nucleon degrees of freedom for s-wave pion production. The tree-level and loop contributions due to the explicit Delta-resonance will be discussed in Secs. III C and III D.

The rescattering operator at LO involves the Weinberg–Tomozawa  $\pi N$  vertex from  $\mathcal{L}_{\pi N}^{(1)}$  and its recoil correction from  $\mathcal{L}_{\pi N}^{(2)}$  which give the resulting operator amplitude:

$$iM_{\text{rescat}}^{\text{LO}} = iM_{\text{WT}}^{\text{LO}} + iM_{\text{WT}}^{\text{recoil}} = \frac{g_A}{2f_\pi^3} \frac{v \cdot q}{k_2^2 - m_\pi^2 + i0} (S_2 \cdot k_2) \tau_X^a + (1 \leftrightarrow 2), \quad (5)$$

where the superscript  $a$  ( $a=1,2,3$ ) here and in what follows refers to the isospin quantum number of the outgoing pion field. The momenta are defined in Fig.4. Further,  $k_2 = p_2 - p'_2$ ,

$v^\mu = (1, \vec{0})$  is the nucleon four-velocity and  $S^\mu$  is its spin-vector, see Appendix B for further details.

The rescattering operator at N<sup>2</sup>LO contains the corrections suppressed as  $1/m_N$  due to the vertices from  $\mathcal{L}_{\pi N}^{(2)}$  and also the corrections  $\propto 1/m_N^2$  from  $\mathcal{L}_{\pi N}^{(3)}$ . We call these amplitude operators  $M_{\text{rescat1}}^{\text{N}^2\text{LO}}$  and  $M_{\text{rescat2}}^{\text{N}^2\text{LO}}$ , respectively. The explicit expressions are:

$$iM_{\text{rescat1}}^{\text{N}^2\text{LO}} = \frac{g_A}{f_\pi^3} \frac{(S_2 \cdot k_2) \tau_2^a}{k_2^2 - m_\pi^2 + i0} \left[ 4c_1 m_\pi^2 - v \cdot q v \cdot k_2 \left( 2c_2 + 2c_3 - \frac{g_A^2}{4m_N} \right) \right] - \frac{g_A}{f_\pi^3} \frac{(v \cdot q) \tau_\times^a}{k_2^2 - m_\pi^2 + i0} \frac{S_2 \cdot (p_2 + p_2')}{4m_N} (v \cdot k_2) + (1 \leftrightarrow 2), \quad (6)$$

$$iM_{\text{rescat2}}^{\text{N}^2\text{LO}} = \frac{g_A}{f_\pi^3} \frac{v \cdot q}{k_2^2 - m_\pi^2 + i0} \left\{ -\tau_2^a (S_2 \cdot k_2) \frac{k_2 \cdot (p_1 + p_1')}{m_N^2} \left( m_N c_2 - \frac{g_A^2}{16} \right) + \tau_\times^a (S_2 \cdot k_2) \left[ \frac{\vec{p}_1^2 + \vec{p}_1'^2}{16m_N^2} + \frac{1 + g_A^2 + 8m_N c_4}{8m_N^2} \left( [S_1 \cdot k_2, S_1 \cdot (p_1 + p_1')] + \frac{k_2^2}{2} \right) \right] - \frac{\tau_\times^a}{8m_N^2} [(S_2 \cdot p_2') p_2^2 - (S_2 \cdot p_2) p_2'^2] \right\} + (1 \leftrightarrow 2), \quad (7)$$

where  $[S_{1\mu}, S_{1\nu}] = S_{1\mu} S_{1\nu} - S_{1\nu} S_{1\mu}$ . The first two terms in the curly bracket in Eq.(7) are due to the corrections to the  $\pi\pi NN$  vertex from  $\mathcal{L}_{\pi N}^{(3)}$  while the last one stands for the correction to the  $\pi NN$  vertex at the same order. Both amplitudes  $M_{\text{rescat1}}^{\text{N}^2\text{LO}}$  and  $M_{\text{rescat2}}^{\text{N}^2\text{LO}}$  contribute to the isoscalar ( $\mathcal{A}$ ) and isovector ( $\mathcal{B}$ ) amplitudes.

In addition to the rescattering operators just derived, one needs to account for the contributions from the direct pion emission from a single nucleon, the so-called direct diagrams which are shown in the first and third rows of Fig.1 and contribute at LO and N<sup>2</sup>LO. Note that in these direct diagrams, the OPE or the  $NN$  contact term, which appear together with the  $\pi NN$  vertex for outgoing pion in Fig.1, will be considered as part of the final (or initial)  $NN$  wave function. In Fig. 4, the OPE and the  $NN$  contact term are, therefore, not shown. After this separation of the  $NN$ -interaction part, the contribution of the ‘‘direct’’ diagrams shown in Fig.4 becomes a one-nucleon operator and can be written as

$$iM_{\text{dir}} = \frac{g_A}{f_\pi} \tau_1^a v \cdot q \delta(\vec{p}_2 - \vec{p}_2') \times \left[ -\frac{1}{2m_N} S_1 \cdot (p_1 + p_1') + \frac{1}{4m_N^2} (v \cdot p_1 (S_1 \cdot p_1) + v \cdot p_1' (S_1 \cdot p_1')) \right] + (1 \leftrightarrow 2) \quad (8)$$

This amplitude contributes to observables only when convoluted with the  $NN$  wave functions. For further discussion see Appendix A.

These LO and N<sup>2</sup>LO operator amplitudes generated by the diagrams in Fig.4 have to be added to the N<sup>2</sup>LO loop diagrams to be presented in Sec. IIC in order to generate the complete N<sup>2</sup>LO s-wave pion-production operator amplitude from pion-nucleon diagrams. We postpone the discussion of the combined s-wave pion-production amplitude until the end of Sec. III where also the  $\Delta$  degrees of freedom will be added to the pion production s-wave amplitude.

### C. Pion-production operator from pion-nucleon loop diagrams up to N<sup>2</sup>LO

The contribution of pion-nucleon loops to the production operator for s-wave pions was derived in Ref. [16] and we just summarize the results:

$$iM_{g_A}^{\text{N}^2\text{LO}} = \frac{g_A (v \cdot q)}{f_\pi^5} \tau_\times^a (S_1 + S_2) \cdot k_1 \left[ \frac{1}{6} I_{\pi\pi}(k_1^2) - \frac{1}{18} \frac{1}{(4\pi)^2} \right], \quad (9)$$

$$iM_{g_A^3}^{\text{N}^2\text{LO}} = \frac{g_A^3 (v \cdot q)}{f_\pi^5} \left\{ \tau_+^a i\varepsilon^{\alpha\mu\nu\beta} v_\alpha k_{1\mu} S_{1\nu} S_{2\beta} [-2I_{\pi\pi}(k_1^2)] \right. \\ \left. + \tau_\times^a (S_1 + S_2) \cdot k_1 \left[ -\frac{19}{24} I_{\pi\pi}(k_1^2) + \frac{5}{9} \frac{1}{(4\pi)^2} \right] \right\}, \quad (10)$$

where the integral  $I_{\pi\pi}(k_1^2)$  is defined in Appendix C<sup>2</sup>. Note that both  $M_{g_A}^{\text{N}^2\text{LO}}$  and  $M_{g_A^3}^{\text{N}^2\text{LO}}$  are proportional to the outgoing pion energy  $v \cdot q \simeq m_\pi$ , i.e. both operator amplitudes vanish at threshold in the chiral limit as expected.

The contributions of the loops to the amplitudes  $\mathcal{A}$  and  $\mathcal{B}$ , see Eq. (2), can be separated into singular and finite parts, where the singular parts are given by the UV divergences appearing in the integral,  $I_{\pi\pi}(k_1^2)$ , in Eqs. (9) and (10).

$$\mathcal{A} = \frac{m_\pi}{(4\pi f_\pi)^2 f_\pi^3} (\tilde{\mathcal{A}}_{\text{singular}} + \tilde{\mathcal{A}}_{\text{finite}}), \\ \mathcal{B} = \frac{m_\pi}{(4\pi f_\pi)^2 f_\pi^3} (\tilde{\mathcal{B}}_{\text{singular}} + \tilde{\mathcal{B}}_{\text{finite}}). \quad (11)$$

The UV divergences are absorbed into LECs accompanying the  $(NN)^2\pi$  amplitudes  $\mathcal{A}_{\text{CT}}$  and  $\mathcal{B}_{\text{CT}}$ , given in the last row in Fig.1. By renormalization, the singular parts of the loop amplitudes are eliminated and we are left with the renormalized finite LECs,  $\mathcal{A}_{\text{CT}}^r$  and  $\mathcal{B}_{\text{CT}}^r$ , which will be added to the finite parts of the loop amplitude operators. Based on the renormalization scheme of Ref. [16], the finite parts of the pion-nucleon loops are

$$\tilde{\mathcal{A}}_{\text{finite}}(\mu) = -\frac{g_A^3}{2} \left[ 1 - \log\left(\frac{m_\pi^2}{\mu^2}\right) - 2F_1\left(\frac{-\vec{p}^2}{m_\pi^2}\right) \right], \\ \tilde{\mathcal{B}}_{\text{finite}}(\mu) = -\frac{g_A}{6} \left[ -\frac{1}{2} \left( \frac{19}{4} g_A^2 - 1 \right) \left( 1 - \log\left(\frac{m_\pi^2}{\mu^2}\right) - 2F_1\left(\frac{-\vec{p}^2}{m_\pi^2}\right) \right) + \frac{5}{3} g_A^2 - \frac{1}{6} \right], \quad (12)$$

where  $\mu$  is the scale and the function  $F_1$  is defined in the appendix, Eq. (C3). In general, as discussed in Ref. [16], the finite parts of the loops  $\tilde{\mathcal{A}}_{\text{finite}}$  and  $\tilde{\mathcal{B}}_{\text{finite}}$  can be further decomposed into the *short-* and *long-range* parts. The former one is just a (renormalization scheme dependent) constant to which all terms in Eq. (12) except  $F_1$  contribute. On the other hand, the long-range part of the loops is scheme-independent. By expanding the function  $F_1(-\vec{p}^2/m_\pi^2)$ , Eq. (C3), which is the only long-range piece in Eq. (12), in the kinematical regime relevant for pion production, i.e.  $(\vec{p}^2/m_\pi^2) \gg 1$ , one obtains up-to-and-including N<sup>2</sup>LO terms

$$\tilde{\mathcal{A}}_{\text{finite}}^{\text{long}} = -\frac{g_A^3}{2} \log\left(\frac{m_\pi^2}{\vec{p}^2}\right) + \mathcal{O}\left(\frac{m_\pi^2}{\vec{p}^2}\right), \\ \tilde{\mathcal{B}}_{\text{finite}}^{\text{long}} = \frac{g_A}{12} \left( \frac{19}{4} g_A^2 - 1 \right) \log\left(\frac{m_\pi^2}{\vec{p}^2}\right) + \mathcal{O}\left(\frac{m_\pi^2}{\vec{p}^2}\right). \quad (13)$$

<sup>2</sup> In Ref. [16], the integral  $I_{\pi\pi}(k_1^2)$  was called  $J(k_1^2)$ .

A numerical evaluation of these terms gives  $\tilde{\mathcal{A}}_{\text{finite}}^{\text{long}} = 2.2$  and  $\tilde{\mathcal{B}}_{\text{finite}}^{\text{long}} = -1.5$ . In Ref. [16] these numbers were compared with those from the most important phenomenological contributions which were proposed in Refs. [26–29] in order to resolve the discrepancy between phenomenological calculations and experimental data. Using the mechanisms suggested in Refs. [26–29], one obtained  $\tilde{\mathcal{A}}_{\text{CT}}^r \simeq 2$  and  $\tilde{\mathcal{B}}_{\text{CT}}^r \simeq 1$  in the same units. Based on this, it was concluded in [16] that the scheme-independent long-range contributions of pion-nucleon loops, not included in the previous studies, are comparable in size with the contribution needed to bring theory in agreement with experiment.

In the next section, Sec.III, we derive the results for N<sup>2</sup>LO loops including the Delta resonance. In particular, it will be shown that the long-range contributions of the pion-nucleon and the Delta loops are of similar size, in agreement with the power counting estimate.

### III. S-WAVE PION PRODUCTION TO N<sup>2</sup>LO: $\Delta$ -RESONANCE INDUCED CONTRIBUTIONS

The threshold pion-production reaction involves energies where the  $\Delta$ -resonance is not heavy enough to be parametrized just by  $\pi N$  LECs. The  $\Delta$  should in fact be explicitly included in the loops as virtual nucleon excitations in order for the effective theory to properly describe the physics in this energy region. Indeed, whereas the mass difference  $\delta$  is non-zero even in the chiral limit of the theory (when  $m_\pi \rightarrow 0$ ), the physical value of  $\delta$ ,  $\delta \approx 300$  MeV, is numerically very close to the “small” scale in the MCS, i.e. the momentum scale  $p \sim \sqrt{m_\pi m_N}$ . Hence, Hanhart and Kaiser [13] argued that, as a practical “consistency” in MCS,  $\delta$  should be counted as  $p$ . In this section we will outline the operator structure due to the inclusion of explicit  $\Delta$  degrees of freedom for the  $NN \rightarrow NN\pi$  reaction.

When the Delta is explicitly included, the LECs  $c_2$ ,  $c_3$  and  $c_4$ , which are determined from pion-nucleon data, have to be re-evaluated. As a consequence, in the Delta-full theory, one obtains the LECs in which the Delta contribution is subtracted. These residual LECs enter the calculation of the pion-production operator derived in Sec. II, see Eqs.(6) and (7). Once we include explicitly the  $\Delta$ -field in the Lagrangian, the parameter  $\delta \sim p$  will appear in loops containing the  $\Delta$  propagator and the resulting loop momentum will naturally be of the order of  $p$ , i.e., these loop diagrams will then contribute at NLO and N<sup>2</sup>LO in the MCS.

In the MCS with a  $\Delta$  explicitly included, we also have to consider loop diagrams with topologies different from those discussed in previous sections. Some of these additional loop diagrams containing a  $\Delta$  propagator will renormalize LO diagram vertices as well as the nucleon wave function. This is in contrast to the loop diagrams with only nucleon and pion propagators, which contribute to renormalization of the vertices at N<sup>4</sup>LO only, as argued in Ref. [16]. This is a higher order than what is considered in this work. These considerations will be explained in detail in the next subsections.

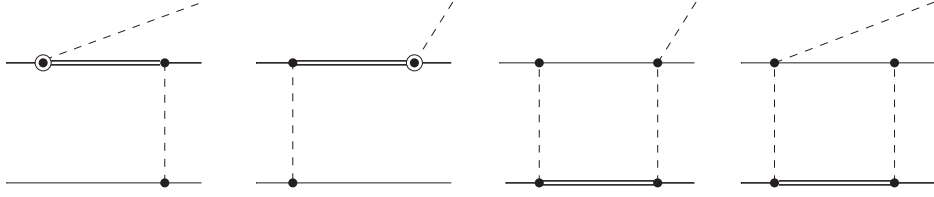


FIG. 5: Reducible  $\Delta$  contributions at NLO (first two diagrams) and at  $N^2$ LO (last two).

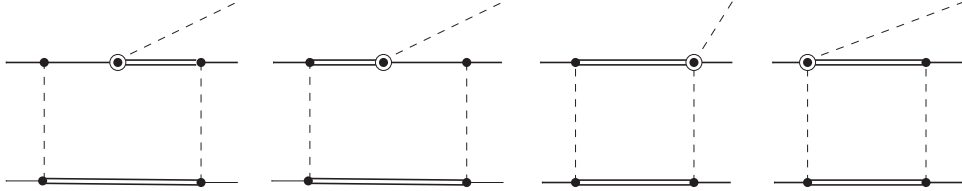


FIG. 6: Examples of  $N^3$ LO contributions involving  $\Delta\Delta$  intermediate states.

### A. The Lagrangian with $\Delta$ interactions

The evaluation of the amplitude contributions involving  $\Delta$  is based on the effective Lagrangian [40, 41] which reads in the  $\sigma$ -gauge

$$\begin{aligned}
\mathcal{L}_{\pi N\Delta} = & -\Psi_{\Delta}^{\dagger}(iv \cdot \partial - \delta)\Psi_{\Delta} + \frac{g_1}{f_{\pi}}\Psi_{\Delta}^{\dagger}\mathbb{S}^{\dagger\mu}S^{\beta}\mathbb{S}_{\mu}T_i\boldsymbol{\tau} \cdot \partial_{\beta}\boldsymbol{\pi}T_i\Psi_{\Delta} \\
& -\frac{1}{4f_{\pi}^2}\Psi_{\Delta}^{\dagger}\left[(\dot{\boldsymbol{\pi}} \times \boldsymbol{\pi}) \cdot T_i^{\dagger}\boldsymbol{\tau}T_i + 2i\left((\mathbf{T}^{\dagger} \cdot \boldsymbol{\pi})(\mathbf{T} \cdot \dot{\boldsymbol{\pi}}) - (\mathbf{T}^{\dagger} \cdot \dot{\boldsymbol{\pi}})(\mathbf{T} \cdot \boldsymbol{\pi})\right)\right]\Psi_{\Delta} \\
& -\frac{h_A}{2f_{\pi}}\left[N^{\dagger}\mathbf{T} \cdot \left(\partial^{\mu}\boldsymbol{\pi} + \frac{1}{2f_{\pi}^2}\boldsymbol{\pi}(\boldsymbol{\pi} \cdot \partial^{\mu}\boldsymbol{\pi})\right)\mathbb{S}_{\mu}\Psi_{\Delta} + h.c.\right] \\
& +\frac{h_A}{2m_N f_{\pi}}\left[iN^{\dagger}\mathbf{T} \cdot \dot{\boldsymbol{\pi}}\mathbb{S} \cdot \partial\Psi_{\Delta} + h.c.\right] + \dots, \tag{14}
\end{aligned}$$

where  $g_1$  is the  $\pi\Delta\Delta$  coupling constant,  $g_1 = 9/5g_A$  from Ref.[42],  $h_A$  is the leading  $\pi N\Delta$  coupling constant and  $\mathbb{S}$  and  $\mathbf{T}$  are the spin and isospin transition matrices, normalized such that

$$\mathbb{S}_{\mu}\mathbb{S}_{\nu}^{\dagger} = g_{\mu\nu} - v_{\mu}v_{\nu} - \frac{4}{1-d}S_{\mu}S_{\nu}, \quad T_iT_j^{\dagger} = \frac{1}{3}(2\delta_{ij} - i\epsilon_{ijk}\tau_k), \quad i, j = 1, 2, 3.$$

An estimate of the  $\pi N\Delta$  coupling constant  $h_A = 2g_{\pi N\Delta} = 3g_A/\sqrt{2} = 2.7$  is derived from large  $N_c$  arguments [43], whereas a determination of  $g_{\pi N\Delta}$  from a fit to the decay width of the  $\Delta$  resonance to leading order in the small-scale expansion gives  $h_A = 2.1$  [41].

### B. Reducible diagrams with $\Delta$ -resonance

The application of the scheme originally proposed by Weinberg [44, 45] to pion-production reactions suggests that the full pion-production amplitude can be evaluated by convolving the pion-production operator, which consists of irreducible graphs only, with  $NN$  wave

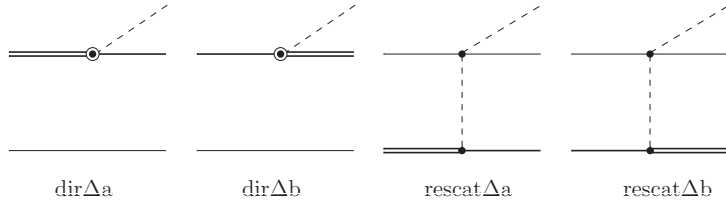


FIG. 7: Single baryon and rescattering diagrams with  $\Delta$  contributions which appear as building blocks in the construction of the pion-production amplitude. In the last two rescattering diagrams only the on-shell part of the  $\pi N$  vertex ( $2m_\pi$ ) from Eq. (4) should be included.

functions in the initial and final states. Only on-shell amplitudes are physically meaningful and can be compared to each other via power counting. To find the MCS order we estimate the order of the diagrams shown in Fig. 5. It is understood that the OPE in the diagrams will in the actual evaluations be considered as a part of the  $NN \rightarrow N\Delta$  amplitude similar to the direct diagrams discussion in Sec. II B. For example, the first diagram in Fig. 5 is suppressed relative to the LO direct one-nucleon diagram in Fig. 1 since the  $\Delta$  propagator is reduced by  $m_\pi/\delta \sim m_\pi/p$  compared to the nucleon one given in Eq. (3). Therefore, this direct  $\Delta$ -diagram in Fig. 5 contributes at NLO. Meanwhile, the reducible box diagrams (the last two) in Fig. 5, which are to be evaluated with the on-shell ( $2m_\pi$ )  $\pi N$  vertex as shown in Eq.(4), start to contribute at N<sup>2</sup>LO. Interestingly, the diagrams in Fig. 6 involving the  $\Delta\Delta$  intermediate state contribute to the on-shell production operator only with subleading vertices at the loop-level and are therefore of a higher order. In particular, a comparison of the box diagrams with one and two  $\Delta$  propagators in Figs. 5 and 6 reveals that the latter are suppressed due to the absence of the  $\pi N \rightarrow \pi\Delta$  vertex at leading order.

Since the  $NN$  and  $N\Delta$  states are coupled in the  $NN$  models [46, 47] which will be used to evaluate the initial and final state  $NN$  wave functions in  $NN \rightarrow NN\pi$ , the full pion-production amplitude also receives contributions from the building blocks containing  $N\Delta$  states as shown in Fig.7. In full analogy to the “direct” single nucleon diagrams in Fig. 1 and as discussed in Sec. II, diagrams shown in Fig. 7 do not contribute to the on-shell pion-production operator but are relevant only when convolved with the  $NN - N\Delta$  amplitude either in the initial or in the final state.

### C. Tree-level diagrams with $\Delta$ -resonance

In this subsection we provide explicit expressions for the contributions of the diagrams in Fig.7, and we obtain the following expressions:

$$\begin{aligned}
iM_{\text{dir}\Delta\text{a}} &= -\frac{g_{\pi N\Delta}}{m_N f_\pi} T_1^a v \cdot q (\mathbb{S}_1 \cdot p_1) \delta(\vec{p}_2 - \vec{p}'_2), \\
iM_{\text{dir}\Delta\text{b}} &= -\frac{g_{\pi N\Delta}}{m_N f_\pi} T_1^{\dagger a} v \cdot q (\mathbb{S}_1^\dagger \cdot p'_1) \delta(\vec{p}_2 - \vec{p}'_2), \\
iM_{\text{rescat}\Delta\text{a}} &= \frac{g_{\pi N\Delta}}{2f_\pi^3} v \cdot q i\epsilon^{bac} \tau_1^c T_2^b \frac{1}{k_2^2 - m_\pi^2 + i0} (\mathbb{S}_2 \cdot k_2), \\
iM_{\text{rescat}\Delta\text{b}} &= \frac{g_{\pi N\Delta}}{2f_\pi^3} v \cdot q i\epsilon^{bac} \tau_1^c T_2^{\dagger b} \frac{1}{k_2^2 - m_\pi^2 + i0} (\mathbb{S}_2^\dagger \cdot k_2).
\end{aligned} \tag{15}$$

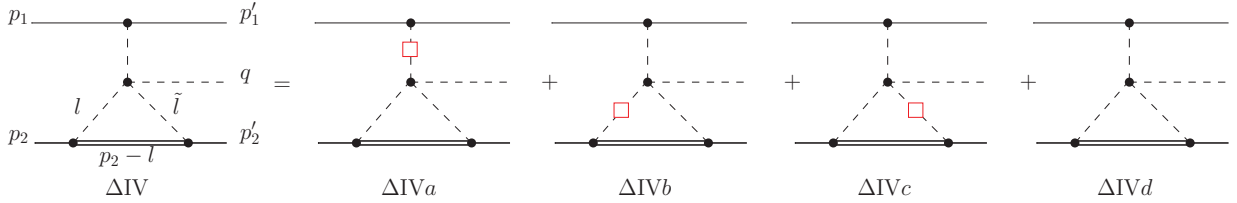


FIG. 8: An example of the loop diagrams with the explicit  $\Delta$ . Double lines denote the  $\Delta$  propagator, remaining notation is as in Fig. 1. The red squares on the pion propagators indicate that for each diagram, the pion propagator cancels parts of the four-pion vertex expression, as explained in the text.

Of course, these tree-level pion-production amplitudes with a  $N\Delta$  initial or final state can not by definition contribute to the  $NN \rightarrow NN\pi$  irreducible production operator. On the other hand, the amplitudes (15) give a nonzero contribution to the full pion-production amplitude when they are inserted as a building block into those of FSI and ISI diagrams which have an  $N\Delta$  intermediate state. The corresponding expressions are given in the Appendix (A), see Eqs. (A2) (A3) and (A4). The contribution of these operators corresponding to charged pion production in  $pp \rightarrow d\pi^+$  was evaluated in Ref. [34].

#### D. Loop diagrams with $\Delta$ propagators

In order to illustrate the power counting of the loop diagrams with  $\Delta$  in MCS we, as an example, discuss in detail the power counting for diagram type  $\Delta IV$  in Fig. 8. First, note that the four-pion vertex of the leftmost diagram in Fig. 8 can be rewritten as a linear combination of the three pion propagators adjacent to this vertex plus a residual vertex term<sup>3</sup> (see, e.g., appendix A.4 in Ref. [16]). This results in a separation of diagram  $\Delta IV$  in four parts: for the diagrams  $\Delta IV$  a-c the pion propagator cancels corresponding parts of the four-pion vertex, as indicated by the red square in Fig. 8, while diagram  $\Delta IV$  d appears as the residual part in this separation. To estimate the magnitudes of the amplitudes of these diagrams, we first remind the reader that for the reaction  $NN \rightarrow NN\pi$  close to threshold the initial nucleons have four-momentum  $p_1^\mu = (m_\pi/2, \vec{p})$  and  $p_2^\mu = (m_\pi/2, -\vec{p})$  with  $p = |\vec{p}| \approx \sqrt{m_\pi m_N}$  (see Fig. 8 for the notation). Secondly, we note that the loop diagrams with the explicit  $\Delta$  all involve the  $\Delta$ - $N$  mass difference  $\delta \sim p$  in the  $\Delta$  propagator. The power counting for the loop diagrams also requires the inclusion of the integral measure  $l^4/(4\pi)^2$  where all components of the loop four-momentum  $l$  are of order  $\delta \sim p$ , i.e.  $v \cdot l \sim |\vec{l}| \sim p$ . In addition to this integral measure, in the diagrams  $\Delta IV$  a-c one has to account for one  $\Delta$  propagator ( $\sim 1/(v \cdot l) \sim 1/p$ ), three pion propagators ( $\sim 1/(p^2)^3$ ), the  $4\pi$  vertex ( $\sim p^2/f_\pi^2$ ) and two  $\pi N\Delta$  and one  $\pi NN$  vertices ( $\sim (p/f_\pi)^3$ ). Combining all these factors and using  $4\pi f_\pi \sim m_N$ , one obtains the order estimate for this diagram as follows

$$\frac{p^4}{(4\pi)^2} \frac{1}{p} \frac{1}{(p^2)^3} \frac{p^2}{f_\pi^2} \left(\frac{p}{f_\pi}\right)^3 \sim \frac{1}{f_\pi^3} \frac{p^2}{m_N^2} \simeq \frac{1}{f_\pi^3} \chi_{\text{MCS}}^2. \quad (16)$$

<sup>3</sup> While the first three terms depend explicitly on the parameterisation (or “gauge”) of the pion field, the residual term is pion-gauge independent [17].

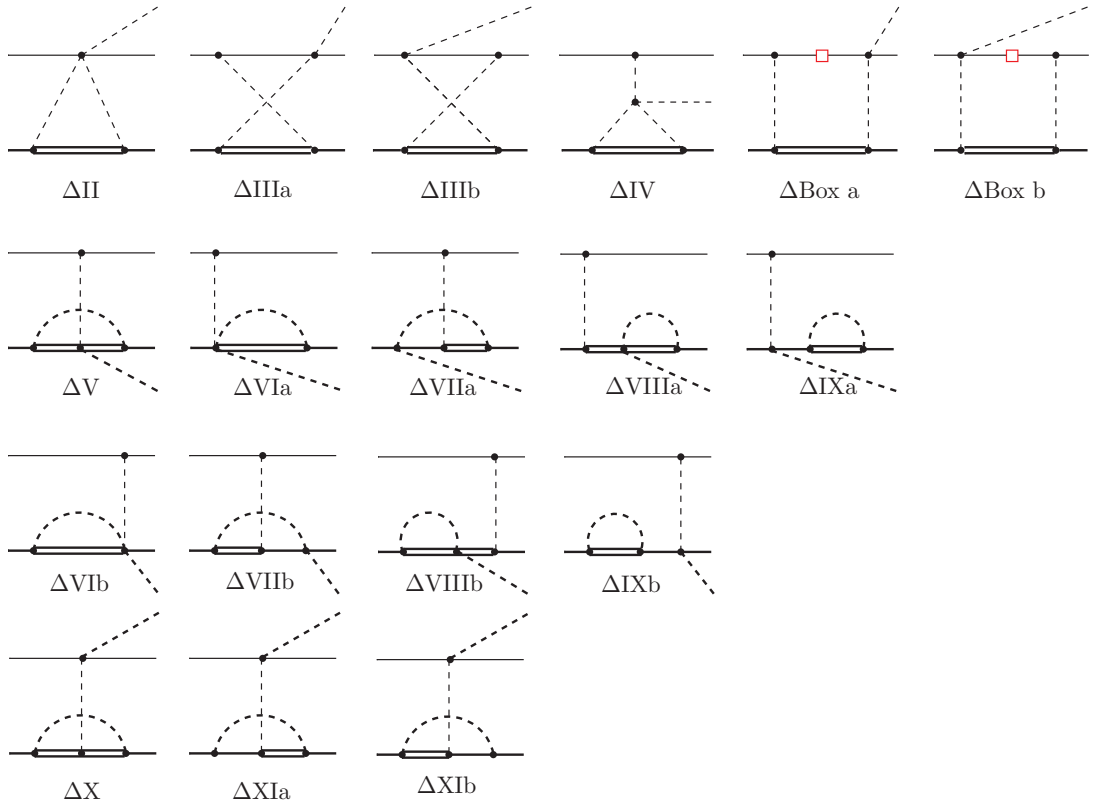


FIG. 9: Loop diagrams with the  $\Delta$  degree of freedom contributing to s-wave pion production up to  $N^2\text{LO}$ . Double lines denote the  $\Delta$  propagator, remaining notation is as in Fig. 1. Again, the red square on the nucleon propagator in the two box diagrams indicates that the corresponding nucleon propagator cancels parts of the Weinberg–Tomozawa  $\pi N$  rescattering vertex leading to an irreducible contribution of the box diagrams as discussed in Sec. II B.

This order estimate of diagrams  $\Delta\text{IVa-c}$  based on dimensional arguments should be compared with the corresponding estimate of a leading-order diagram for the  $NN \rightarrow NN\pi$  reaction, namely the rescattering diagram with the Weinberg–Tomozawa vertex, as given by Eq.(3). Thus, we find that the diagrams  $\Delta\text{IVa-c}$  in Fig. 8 start to contribute at NLO. Meanwhile, the pion-gauge independent diagram  $\Delta\text{IV d}$  starts to contribute at  $N^2\text{LO}$  only. The reason is that the residual pion-gauge independent  $4\pi$  vertex is suppressed compared to the leading  $4\pi$  contributions. Finally, notice that the expression for diagram  $\Delta\text{IV}$  contains more terms than the corresponding pure pion-nucleon diagram IV. In the pion-nucleon case, the contributions similar to type  $\Delta\text{IVb}$  and  $\Delta\text{IVc}$  are strongly suppressed since they involve only the momentum scale of the order of  $m_\pi$ , as explained in Appendix A.4 in Ref. [16].

The loop diagrams involving  $\Delta$  which contribute to s-wave pion production up to  $N^2\text{LO}$  are shown in Fig. 9. In the first row of Fig. 9, we have the two-pion exchange diagrams with topologies completely analogous to the pion-nucleon  $g_A^3$ -graphs in the second row in Fig. 1. The two-pion exchange diagrams in the first row of Fig. 9 individually start to contribute at NLO. However, these NLO diagrams cancel completely in the sum for the same reason as do the NLO pion-nucleon ones in Fig. 1. In fact, it is relatively straightforward to show that, on the operator level, this cancellation of the NLO level diagrams is independent of whether we have a nucleon or a  $\Delta$  propagator on the lower baryon line in Figs. 1 and 9. Consequently, in

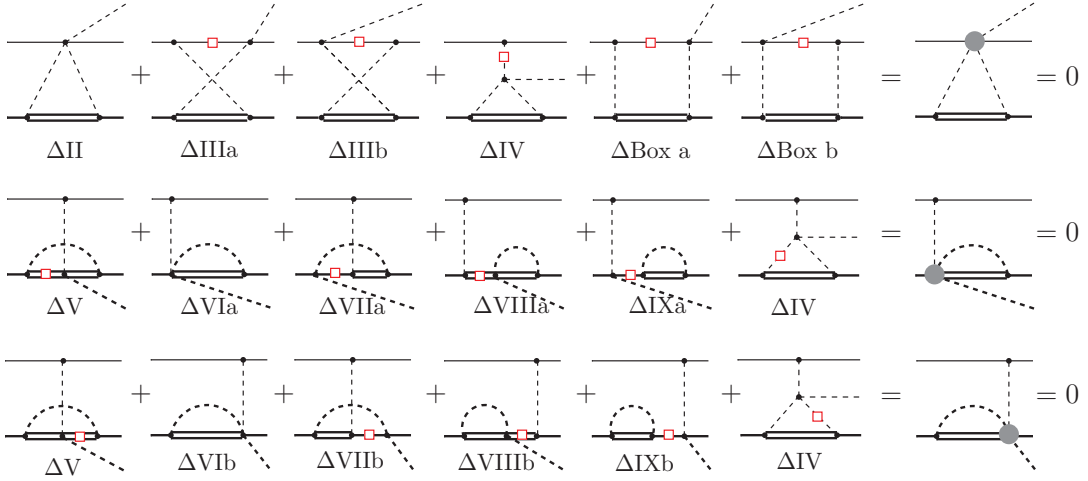


FIG. 10: Illustration of the cancellation pattern among the  $\Delta$ -loop contributions for different topologies shown on the l.h.s. of each row. The red squares on the nucleon or  $\Delta$  propagators indicate that for each diagram this nucleon or  $\Delta$  propagator cancels parts of the adjacent  $\pi N$  or  $\pi\Delta$  rescattering vertex. The red squares on the pion propagators indicate that for each diagram the pion propagator cancels parts of the four-pion vertex expression. These propagator cancellations generate the rightmost effective diagrams in each row where the effective vertices (blobs) receive contributions from all the diagrams on the l.h.s. in the corresponding row. The zero on the very r.h.s. in each row means that the sum of all diagrams on the l.h.s. contributes nothing to the s-wave pion production at least up to  $N^2\text{LO}$ .

MCS there are no contributions from these two-pion exchange diagrams at NLO. Moreover, the  $N^2\text{LO}$  contributions of the diagrams in the first row in Fig. 9 also show cancellation patterns among the diagrams absolutely analogous to the purely pion-nucleon case. In the first row of Fig. 10, we demonstrate graphically this systematic cancellation pattern of these diagrams at NLO and  $N^2\text{LO}$ , where a nucleon (pion) propagator cancels parts of a Weinberg-Tomozawa  $\pi N$  rescattering (four-pion) vertex expression, rendering an effective diagram of topology like diagram  $\Delta\text{II}$  but with an effective three-pion-nucleon vertex which vanishes. It should be mentioned that the diagrams in the first row of Fig. 9 also obtain corrections from higher-order vertices  $\propto 1/m_N$  and  $c_i$  (Delta-subtracted) from  $\mathcal{L}_{\pi N}^{(2)}$ . Those corrections, however, again cancel completely at  $N^2\text{LO}$  in a full analogy to the cancellations among the corresponding pion-nucleon loop contributions, see Ref. [16] and the discussion in Sec.II C. The net sum of the  $N^2\text{LO}$  diagrams in the first row of Fig. 9 receives contributions only from diagrams  $\Delta\text{IIIa}$  and  $\Delta\text{IIIb}$ , where the Weinberg-Tomozawa  $\pi N$  vertices are on-shell, and a remnant of diagram  $\Delta\text{IV}$ , the pion-gauge independent  $\Delta\text{IVd}$  shown in Fig. 8. In other words, the contributions of the diagrams  $\Delta\text{IVa-c}$  in Fig. 8 cancel against other diagrams, as indicated in Fig. 10, and only  $\Delta\text{IVd}$  with a residual part of the four-pion vertex remains.

In addition, there are several new loop diagrams containing  $\Delta$  propagators where one effectively has a pion being exchanged between the two nucleons, see diagrams  $\Delta\text{V}-\Delta\text{XI}$  in Fig. 9. Surprisingly, parts of diagrams  $\Delta\text{V}-\Delta\text{IX}$  in rows two and three also undergo significant cancellations. Again, as illustrated in rows two and three in Fig. 10, after the cancellations of the vertex structures with the propagators, some parts of the diagrams  $\Delta\text{V}-\Delta\text{IX}$  and  $\Delta\text{IV}$  acquire the effective topology of the diagrams  $\Delta\text{VIa}$  and  $\Delta\text{VIb}$ . The net

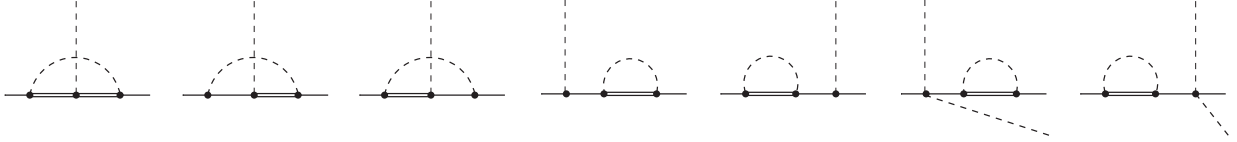


FIG. 11: Various renormalization diagrams relevant at N<sup>2</sup>LO. The first three diagrams contribute to the renormalization correction of the  $\pi N$  coupling constant  $g_A$ , whereas the last four diagrams renormalize the nucleon wave function using the leading vertices in the theory with explicit  $\Delta$  degrees of freedom.

effect of such contributions again vanishes at NLO and N<sup>2</sup>LO for s-wave pion production as indicated on the r.h.s. in rows two and three of Fig. 10. After the cancellations, only those parts of diagrams  $\Delta V$ – $\Delta IX$  remain, that are proportional to the on-shell part,  $2m_\pi$ , of the  $\pi\Delta - \pi\Delta$  and  $\pi N - \pi N$  vertices. Although the dimensional analysis estimate indicates that these residual contributions are naively of N<sup>2</sup>LO in MCS, most of the N<sup>2</sup>LO amplitude expression vanishes due to loop angular integration. For example, for diagrams  $\Delta VII$  the numerator of the integrand  $\propto 2m_\pi \mathbb{S} \cdot (p_1 - p'_1)(\mathbb{S} \cdot l)$  is odd with the loop momentum  $l$  yielding the vanishing contribution at N<sup>2</sup>LO. As a consequence of these cancellations almost all loop diagrams in rows two and three in Fig. 9 do not contribute to the s-wave N<sup>2</sup>LO pion-production amplitude. Only diagram  $\Delta V$  in the second row yields a non-vanishing N<sup>2</sup>LO contribution from the loop diagrams in rows two and three, where again only the on-shell part of the  $\pi\Delta - \pi\Delta$  rescattering vertex in diagram  $\Delta V$  remains.

Finally, the three one-pion-exchange  $\Delta$  loop diagrams in the last row of Fig. 9, which have to be taken into account at N<sup>2</sup>LO, contribute only to the renormalization of  $g_A$  at N<sup>2</sup>LO, see the next subsection. Furthermore, the time-dependent Weinberg–Tomozawa  $\pi N$  vertex in these three diagrams appears on-shell as discussed in the text after Eq.(4).

### E. Regularization of UV divergences and renormalization

The loop diagrams with explicit  $\Delta$  are UV-divergent at N<sup>2</sup>LO. These  $\Delta$  loop diagrams require that the couplings and masses appearing in the Lagrangian should be renormalized. In particular, up to N<sup>2</sup>LO in MCS we concentrate on two relevant renormalization corrections, namely the ones to the  $\pi N$  coupling constant  $g_A$  and the nucleon wave function renormalization factor  $Z_N$ , as shown in Fig.11. These renormalization corrections of order  $\delta^2/\Lambda_\chi^2 \sim \chi_{\text{MCS}}^2$  were evaluated in Ref. [37, 38] for  $\pi N$  scattering with explicit  $\Delta$  in the loop using dimensional regularization. We confirm the results of Ref. [37, 38, 48]:

$$Z_N = 1 + 2(d-2)g_{\pi N\Delta}^2 \frac{\delta}{f_\pi^2} J_{\pi\Delta} + \mathcal{O}\left(\frac{m_\pi^2}{\Lambda^2}\right), \quad (17)$$

$$\hat{g}_A = g_A + \frac{10(6+d-4d^2+d^3)}{9(d-1)^2} g_1 g_{\pi N\Delta}^2 \frac{\delta}{f_\pi^2} J_{\pi\Delta} + \frac{16(d-2)}{3(d-1)^2} g_A g_{\pi N\Delta}^2 \frac{\delta}{f_\pi^2} J_{\pi\Delta} + \mathcal{O}\left(\frac{m_\pi^2}{\Lambda^2}\right),$$

where  $\hat{g}_A$  is the bare axial coupling,  $g_{\pi N\Delta} = h_A/2$  and  $g_1 = 9/5g_A$  is the  $\pi\Delta\Delta$  coupling constant. In order to calculate the production operator up to NLO it suffices to use  $Z_N = 1$  and  $\hat{g}_A = g_A$ . However, in a theory with explicit  $\Delta$  degrees of freedom, renormalization corrections to the tree-level diagrams at LO in Fig. 1 generate N<sup>2</sup>LO contributions. At

N<sup>2</sup>LO, the nucleon fields ( $N$ ) in the Lagrangian must be renormalized, i.e.,  $N \rightarrow N\sqrt{Z}$ , and, similarly, for the axial constant  $\dot{g}_A \rightarrow g_A$  (i.e.,  $\dot{g}_A$  deviates from the physical value), due to the loop corrections with explicit  $\Delta$  in Eq. (18). The explicit evaluations of the diagrams in Fig. 9 reveal that the contributions of diagrams  $\Delta X$  and  $\Delta XI$  reproduce the N<sup>2</sup>LO correction to the tree-level rescattering diagram in Fig. 1 due to renormalization of  $\dot{g}_A$  and  $Z_N$  (see first five diagrams in Fig.11), meaning that at N<sup>2</sup>LO there is no genuine contributions of diagrams  $\Delta X$  and  $\Delta XI$  in MCS.

The N<sup>2</sup>LO contribution from  $Z_N$  to the WT vertex (the last two diagrams in Fig.11), is included in the rescattering operator together with the residual contributions of the diagrams  $\Delta III$ ,  $\Delta IV$  and  $\Delta V$  and gives non-vanishing correction at N<sup>2</sup>LO. The individual non-vanishing contributions of the  $\Delta$  loop diagrams in Fig. 9, expressed in terms of four well-known scalar integrals,  $J_{\pi\Delta}$ ,  $I_{\pi\pi}$ ,  $J_{\pi\pi\Delta}$ , and  $J_{\pi\pi N\Delta}$ , which are defined in appendix C, Eqs. (C1)–(C6), read

$$\begin{aligned}
iM_{\Delta III(a+b)} &= i(SI_1) \frac{1}{(d-1)(d-2)} \left\{ I_{\pi\pi} - \frac{1}{2} \frac{J_{\pi\Delta}}{\delta} + \delta J_{\pi\pi\Delta} + \frac{1}{4} k_1^2 J_{\pi\pi N\Delta} \right\} \\
&+ i(SI_2) \frac{d-2}{d-1} \left\{ \frac{1}{2} I_{\pi\pi} - \frac{1}{2} \frac{J_{\pi\Delta}}{\delta} + \frac{1}{2} \delta J_{\pi\pi\Delta} + \frac{1}{4} k_1^2 J_{\pi\pi N\Delta} \right\}, \\
iM_{\Delta IV} &= i(SI_2) \frac{d-2}{d-1} \left\{ \left( 2 - \frac{1}{d-1} + 4 \frac{\delta^2}{k_1^2} \right) I_{\pi\pi} - 4 \frac{\delta^2}{k_1^2} \frac{J_{\pi\Delta}}{\delta} + \left( 2 + 4 \frac{\delta^2}{k_1^2} \right) \delta J_{\pi\pi\Delta} \right\}, \\
iM_{\Delta V} &= i(SI_2) (d-2) \left\{ 5 \frac{\delta^2}{k_1^2} \frac{J_{\pi\Delta}}{\delta} \right\}, \\
iM_{\Delta}^{ZN} &= i(SI_2) (d-2) \left\{ -3 \frac{\delta^2}{k_1^2} \frac{J_{\pi\Delta}}{\delta} \right\}, \tag{18}
\end{aligned}$$

where the two spin-isospin operators in Eq.(18) are:

$$\begin{aligned}
(SI_1) &= (-i) \frac{g_{\pi N\Delta}^2}{f_\pi^5} g_A \left\{ \left( \frac{2}{3} \tau_1^a - \frac{1}{3} \tau_2^a \right) 4 [S_{2\mu}, S_{2\nu}] S_1^\nu k_1^\mu v \cdot q + (1 \leftrightarrow 2) \right\}, \\
(SI_2) &= (-i) \frac{g_{\pi N\Delta}^2}{f_\pi^5} g_A \frac{i}{3} \{ (\boldsymbol{\tau}_1 \times \boldsymbol{\tau}_2)^a S_1 \cdot k_1 v \cdot q + (1 \leftrightarrow 2) \}. \tag{19}
\end{aligned}$$

The four different loop integrals in Eq. (18) can be characterized in the following manner. The integral  $J_{\pi\pi\Delta}$ , Eq. (C5), contains two pion propagators and a  $\Delta$  propagator whereas the integral  $J_{\pi\pi N\Delta}$ , Eq. (C6), has an additional nucleon propagator. Furthermore, we note that both of these integrals are UV finite. Meanwhile, the integrals  $J_{\pi\Delta}$  and  $I_{\pi\pi}$  contain UV divergences and, similar to the pion-nucleon loops, some of these divergencies can be absorbed by the five-point  $NN \rightarrow NN\pi$  contact term, see the last row in Fig.1.

Before we present the final transition amplitude contribution for s-wave pion production from  $\Delta$  loop diagrams, there is one issue which deserves attention. In a theory containing a ‘‘heavy’’ resonance  $\Delta$ , it is not sufficient to require just the cancellation of the UV divergent terms with the corresponding LECs. The integrals  $J_{\pi\Delta}$  and  $I_{\pi\pi}$  in Eq. (18) which are multiplied by the factor  $\delta^2/k_1^2$  pose an additional problem. Such polynomial behavior would give divergences if the  $\Delta$ -resonance was infinitely heavy, i.e., if  $\delta \rightarrow \infty$ . Therefore, to find the most natural finite values of the renormalized LECs, the explicit ‘‘decoupling’’ renormalization scheme was introduced [49]. In such a scheme, the finite parts of LECs are chosen such that the renormalized contribution from diagrams with  $\Delta$  loops vanish in the

limit  $\delta \rightarrow \infty$ . It is demonstrated in Appendix C2 that the following combinations of loop integrals (up to N<sup>2</sup>LO in MCS) do vanish when  $\delta \rightarrow \infty$ :

$$k_1^2 J_{\pi\pi N\Delta}, \quad (20)$$

$$\left( I_{\pi\pi} + \frac{1}{2} \frac{J_{\pi\Delta}}{\delta} + \delta J_{\pi\pi\Delta} + \frac{2}{(4\pi)^2} \right), \quad (21)$$

$$\frac{\delta^2}{k_1^2} \left( I_{\pi\pi} + \frac{1}{2} \frac{J_{\pi\Delta}}{\delta} + \delta J_{\pi\pi\Delta} + \frac{2}{(4\pi)^2} \right) - \frac{1}{12} \left( I_{\pi\pi} + \frac{1}{2} \frac{J_{\pi\Delta}}{\delta} + \frac{1}{3} \frac{2}{(4\pi)^2} \right). \quad (22)$$

We find that the combination of the two integrals  $J_{\pi\Delta}$  and  $I_{\pi\pi}$  in Eqs. (20)-(22),  $I_{\pi\pi} + \frac{1}{2\delta} J_{\pi\Delta}$ , cancels the UV divergences of the individual integrals, as proven at the end of the Appendix C2. Hence, Eqs. (20)-(22) are all UV finite and vanish when  $\delta \rightarrow \infty$ .

Rewriting the sum of the amplitudes  $M_{\Delta\text{III}(a+b)}$ ,  $M_{\Delta\text{IV}}$ ,  $M_{\Delta\text{V}}$  and  $M_{\Delta}^{ZN}$  from Eq. (18) in terms of the integral combinations (20)–(22), we obtain the following transition amplitude from the  $\Delta$  loop diagrams

$$\begin{aligned} iM_{\Delta\text{-loops}}^{\text{N}^2\text{LO}} &= \frac{g_A g_{\pi N\Delta}^2}{f_\pi^5} v \cdot q \tau_+^a \left( i\varepsilon^{\alpha\mu\nu\beta} v_\alpha k_{1\mu} S_{1\nu} S_{2\beta} \right) \\ &\times \left\{ \frac{2}{9} \left( I_{\pi\pi} + \frac{1}{2} \frac{J_{\pi\Delta}}{\delta} + \delta J_{\pi\pi\Delta} + \frac{2}{(4\pi)^2} \right) + \frac{1}{18} k_1^2 J_{\pi\pi N\Delta} - \left[ \frac{2}{3(d-1)} \frac{J_{\pi\Delta}}{\delta} \right] + \tilde{\mathcal{A}}_{\text{CT}}^\Delta \right\} \\ &+ \frac{g_A g_{\pi N\Delta}^2}{f_\pi^5} v \cdot q \tau_\times (S_1 + S_2) \cdot k_1 \\ &\times \left\{ \frac{5}{9} \left( I_{\pi\pi} + \frac{1}{2} \frac{J_{\pi\Delta}}{\delta} + \delta J_{\pi\pi\Delta} + \frac{2}{(4\pi)^2} \right) + \frac{1}{18} k_1^2 J_{\pi\pi N\Delta} - \frac{2}{27} \left( I_{\pi\pi} + \frac{1}{2} \frac{J_{\pi\Delta}}{\delta} + \frac{1}{3} \frac{2}{(4\pi)^2} \right) \right. \\ &\left. + \frac{8}{9} \frac{\delta^2}{k_1^2} \left( I_{\pi\pi} + \frac{1}{2} \frac{J_{\pi\Delta}}{\delta} + \delta J_{\pi\pi\Delta} + \frac{2}{(4\pi)^2} \right) - \left[ \frac{(d-2)}{3(d-1)} \left( \frac{19}{12} \frac{J_{\pi\Delta}}{\delta} + \frac{5}{(4\pi)^2} \right) \right] + \tilde{\mathcal{B}}_{\text{CT}}^\Delta \right\}. \quad (23) \end{aligned}$$

Additional terms, that do not vanish at the large  $\delta$  limit, shown in the square brackets in Eq. (23), are short-ranged and are cancelled in the amplitude expression by the parts of the five-point contact terms  $\tilde{\mathcal{A}}_{\text{CT}}^\Delta$  and  $\tilde{\mathcal{B}}_{\text{CT}}^\Delta$  due to the explicit  $\Delta$ . In other words, the decoupling condition fixes the magnitude of the five-point contact interactions due to the explicit  $\Delta$ ,  $\tilde{\mathcal{A}}_{\text{CT}}^\Delta$  and  $\tilde{\mathcal{B}}_{\text{CT}}^\Delta$ , up to higher order terms. In fact, by defining the five point contact terms as

$$\tilde{\mathcal{A}}_{\text{CT}}^\Delta = \frac{2}{3(d-1)} \frac{J_{\pi\Delta}}{\delta} + O\left(\frac{m_\pi^2}{\delta^2}\right), \quad (24)$$

$$\tilde{\mathcal{B}}_{\text{CT}}^\Delta = \frac{(d-2)}{3(d-1)} \left( \frac{19}{12} \frac{J_{\pi\Delta}}{\delta} + \frac{5}{(4\pi)^2} \right) + O\left(\frac{m_\pi^2}{\delta^2}\right), \quad (25)$$

we obtain the fully renormalized, finite  $\Delta$  loops amplitude contribution, which satisfies the

decoupling condition, to s-wave pion production at N<sup>2</sup>LO:

$$\begin{aligned}
iM_{\Delta\text{-loops}}^{\text{N}^2\text{LO}} &= \frac{g_A g_{\pi N \Delta}^2}{f_\pi^5} v \cdot q \tau_+^a (i\varepsilon^{\alpha\mu\nu\beta} v_\alpha k_{1\mu} S_{1\nu} S_{2\beta}) \\
&\times \left\{ \frac{2}{9} \left( I_{\pi\pi} + \frac{1}{2} \frac{J_{\pi\Delta}}{\delta} + \delta J_{\pi\pi\Delta} + \frac{2}{(4\pi)^2} \right) + \frac{1}{18} k_1^2 J_{\pi\pi N\Delta} \right\} \\
&+ \frac{g_A g_{\pi N \Delta}^2}{f_\pi^5} v \cdot q \tau_\times (S_1 + S_2) \cdot k_1 \\
&\times \left\{ \frac{5}{9} \left( I_{\pi\pi} + \frac{1}{2} \frac{J_{\pi\Delta}}{\delta} + \delta J_{\pi\pi\Delta} + \frac{2}{(4\pi)^2} \right) + \frac{1}{18} k_1^2 J_{\pi\pi N\Delta} \right. \\
&\left. + \frac{8}{9} \frac{\delta^2}{k_1^2} \left( I_{\pi\pi} + \frac{1}{2} \frac{J_{\pi\Delta}}{\delta} + \delta J_{\pi\pi\Delta} + \frac{2}{(4\pi)^2} \right) - \frac{2}{27} \left( I_{\pi\pi} + \frac{1}{2} \frac{J_{\pi\Delta}}{\delta} + \frac{1}{3} \frac{2}{(4\pi)^2} \right) \right\}. \quad (26)
\end{aligned}$$

This expression should be added to the finite s-wave production operators presented in Sec. II.

#### IV. COMPARISON OF THE PION-NUCLEON AND $\Delta$ LOOP CONTRIBUTIONS

In Ref. [16] (see also discussion in Sec. II) we argued that the long-range scheme-independent part of the pion-nucleon loops at N<sup>2</sup>LO is sizable and could resolve the problem with the description of pion production data in the neutral channel,  $pp \rightarrow pp\pi^0$ . We now add the long-ranged  $\Delta$  contribution. First, we note that the spin-isospin structure of the  $\Delta$ -loops in Eq. (26) is exactly the same as for the pion-nucleon case in Eq. (10). Meanwhile, the dimensionless integrals are different and the coefficients in front of the spin-isospin operators also differ. We want to compare the resultant amplitudes from the nucleon and  $\Delta$  loop diagrams for  $NN$  relative distances relevant for pion production, i.e. for  $r \sim 1/p \simeq 1/\sqrt{m_\pi m_N}$ . In order to separate the long-range scheme-independent contributions of the  $\Delta$ -loop expressions from the short-range ones in a transparent manner, we make a Fourier transformation of our expressions. The Fourier transformation of a short-range (constant) contribution gives a  $\delta$ -function,  $\delta(\mathbf{r})$ , which does not influence the long-range physics of interest and we therefore ignore this contribution in this section. The Fourier transformation of the long-range part of the loop integrals is evaluated numerically as follows:

$$I(r) = \int \frac{d^3k}{(2\pi)^3} e^{i\mathbf{k}\mathbf{r}} I(k) e^{-k^2/\Lambda^2}. \quad (27)$$

Here, the regulator  $e^{-k^2/\Lambda^2}$  is used in order to minimize the influence of the large momenta in the loop integrals, denoted by  $I(k)$  for short. We have verified that for  $\Lambda > 2$  GeV this regulator does not affect the results in the long-range region of  $r \sim 1/p$ . Specifically, we Fourier transform the integral combinations in the curly brackets in Eq. (26) (multiplied by  $g_A g_{\pi N \Delta}^2$ ) corresponding to  $\tau_+$  (neutral) and  $\tau_\times$  (charged) channels. We compare the resulting Fourier transformed amplitudes with the Fourier transformed amplitudes of the corresponding pion-nucleon contributions in Eqs. (9) and (10),  $-2g_A^3 I_{\pi\pi}$  and  $(-19/24g_A^3 + 1/6g_A) I_{\pi\pi}$ , respectively. The ratio of the  $r$ -space  $\Delta$  loop contributions to those of the nucleon is shown in Fig. 12. One can see that in the neutral channel, the long-range part of the  $\Delta$

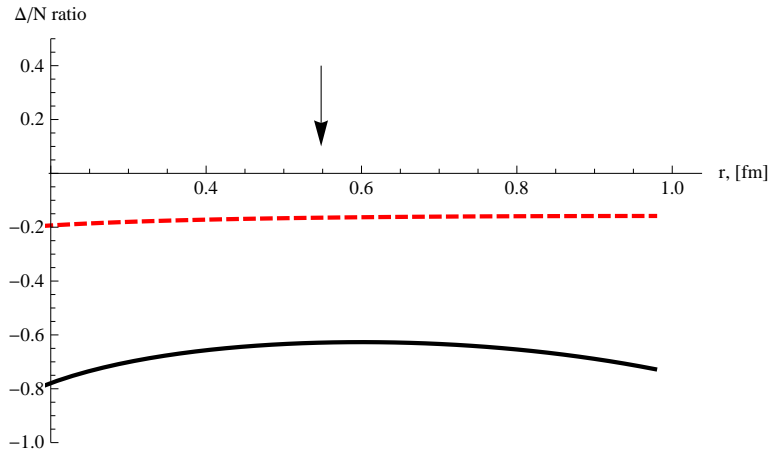


FIG. 12: The ratio of the  $\Delta$  contributions to the pion-nucleon ones for  $\tau_+$  (red dashed curve) and  $\tau_\times$  (black solid curve) channels. The arrow indicates  $r \sim 1/p = 1/\sqrt{m_\pi m_N}$ .

contribution constitutes less than 20% compared to the pion-nucleon loop amplitude. This can be understood by the specific combination of the coefficients for the spin-isospin operator in the case of the  $\Delta$ -resonance amplitude, which results in a suppression by almost one order of magnitude. Therefore, the conclusion of Ref. [16], regarding the importance of the pion-nucleon loops in explaining the neutral pion production, appears to be only slightly modified by the  $\Delta$  loop contributions. Regarding the charged channel the  $\Delta$ -loop contribution to the s-wave pion-production amplitude is almost of the same magnitude (roughly 60%) but of opposite sign compared to the pion-nucleon one. The net loop amplitude from the nucleon and  $\Delta$  loop diagrams is therefore not as important as in the neutral channel.

The pattern that emerged from the loops is therefore exactly what is necessary to quantitatively describe the data on both  $pp \rightarrow pp\pi^0$  and  $pp \rightarrow d\pi^+$  very near threshold: while in the former reaction there persists a huge discrepancy between data and the chiral perturbation theory calculation to NLO, in the latter at NLO the description is already quite good [14]. In line with this we now find that due to large cancellations amongst the pion-nucleon and the Delta loops the N<sup>2</sup>LO corrections from the loops are small in the charged pion channel. On the other hand, this cancellation is by far not that efficient in the neutral pion channel leading to a significant loop contribution. In combination with the observation that in the neutral pion channel the leading order diagrams are suppressed both kinematically as well as dynamically [3], this provides a dynamical reason of why it was so much harder to understand phenomenologically the neutral pion production compared to the charged pion production.

## V. SUMMARY AND CONCLUSIONS

We have investigated the pion production operator in  $NN \rightarrow NN\pi$  near threshold within chiral EFT. Specifically, by explicit inclusion of the Delta-isobar and the  $1/m_N^2$ -corrections we have calculated the pion production operator to next-to-next-to-leading order (N<sup>2</sup>LO) in the momentum counting scheme (MCS). The MCS keeps track of the large initial momenta necessary in order to produce a pion from two nucleons. The MCS approach accounts for the scales encountered in this reaction, namely the pion mass, the intermediate momentum

scale  $p \sim \sqrt{m_\pi m_N}$  compared to the hadronic scale  $\Lambda_\chi$ . An understanding of such a two-scale problem is important also for other systems: e.g. to formulate a power counting for the decays of heavy charmonia via meson loops it is necessary to keep track of various energy and momentum scales [50].

While all loops cancel at NLO, at N<sup>2</sup>LO there is a finite remainder of the  $\Delta$  loop contributions which is of the same order of magnitude as its purely pion-nucleon counter part calculated in Ref. [16]. This finding confirms the conjecture that the new scale introduced by the Delta-nucleon mass splitting should be treated at the same order as the one from the initial momentum.

It is encouraging to observe that the sum of pion-nucleon and Delta loops shows exactly the pattern required by the data. In the channel where there is an isoscalar  $NN$  pair in the final state, there is a large cancellation between the N<sup>2</sup>LO Delta loops and the pion-nucleon ones as indicated in Fig 12. Note that in this channel the NLO calculation of Ref. [14] was already close to reproducing the data. On the other hand, in the channel where the final state  $NN$  pair is in an isovector state the Delta loop contributions are much reduced compared to the pion-nucleon loops as seen in Fig 12. This means that the sum of Delta- and nucleon-loop contributions is sizable and it is precisely in this channel where earlier calculations revealed huge deviations from data.

This indicates that the large quantitative difference between the two near threshold amplitudes  $\mathcal{A}$  and  $\mathcal{B}$  in Eq (2) can be well understood on dynamical grounds based on nucleon, Delta and pion degrees of freedom. Meanwhile, the short-ranged physics contribution is parametrized by local contact terms in effective field theories, and these LECs might well give similar contributions in the two channels. However, in order to make this finding more quantitative, a convolution with proper  $NN$  wave functions is necessary. Formally, in a consistent chiral EFT calculation one should derive the transition operators and the initial and final nucleon wave functions from the same effective Lagrangian. This has not yet been carried out and is beyond the scope of this work. For pragmatic reasons we will consider the hybrid approach where, as in this work, the transition amplitudes are evaluated in ChPT, whereas the nucleon wave functions are generated by modern phenomenological  $NN$  potentials. As a next step, the calculation of observables in the hybrid approach and the comparison with experimental data will be presented in a subsequent work. The intrinsic scheme-dependence inherent to the hybrid approach also needs to be quantified.

Our work provides an important step forward towards understanding the important class of reactions, namely the first inelastic  $NN$  reactions —  $NN \rightarrow NN\pi$ . Especially, it confirms the observation of Ref. [16], where it was pointed out that the long-range physics is not described properly in earlier phenomenological calculations [26–32]. Indeed, none of the loop contributions with nucleons and Delta that survived the significant cancellations, like the pion crossed boxes (cf. diagrams IIIa and IIIb in Figs. 1 and 9), were included in these works. In addition, similar to cancellations among the pion-nucleon loop terms, also all the Delta loops that can be associated with scalar-isoscalar  $\pi N$  interaction in the pion rescattering term cancel. This cancellation is in conflict with the claims of Refs. [30, 31], where these diagrams provided the essential contributions necessary to describe the data.

## Acknowledgments

This work was supported in part by funds provided by the EU HadronPhysics3 project “Study of strongly interacting matter”, the European Research Council (ERC-2010-StG

## Appendix A: Reaction amplitude

In the most general case, an amplitude corresponding to the matrix element of a particular production and/or absorption operator between two-nucleon states with given initial  $(j, l, s)$  and final  $(j', l', s')$  total angular momentum of a nucleon pair, its orbital momentum and total spin<sup>4</sup> is written as

$$\mathcal{M}^{\text{full}}[jls, j'l's'] = \mathcal{M}^{\text{prod}}[jls, j'l's'] + \mathcal{M}^{\text{FSI}}[jls, j'l's'] + \mathcal{M}^{\text{ISI}}[jls, j'l's'] + \mathcal{M}^{\text{ISI+FSI}}[jls, j'l's'] \quad (\text{A1})$$

Here  $\mathcal{M}^{\text{prod}}[jls, j'l's'](p, p')$ , with  $p$  and  $p'$  being the initial and final nucleon relative momenta, stands for the  $NN \rightarrow NN\pi$  production amplitude where there is no  $NN$  interaction in the initial and in the final state, and  $\mathcal{M}^{\text{FSI}}$ ,  $\mathcal{M}^{\text{ISI}}$ ,  $\mathcal{M}^{\text{ISI+FSI}}$  refer to the amplitudes with final state, initial state, and both final and initial state interaction included, in order. In this equation we imply that the spin-angular part (as well as the isospin part) of the amplitudes are factored out. Note that since there is a third particle that carries angular momentum, the pion, the total angular momentum  $j$  of the initial two-nucleon state can be different from that of the final two-nucleon state,  $j'$ . Obviously, the total angular momentum of the final particles equals that of the initial one. The pion-production amplitude for off-shell kinematics ( $\tilde{\mathcal{M}}^{\text{prod}}$ ) includes, in addition to  $\mathcal{M}^{\text{prod}}$ , the single-nucleon (the direct diagrams) production operator Eq. (8) as well as the tree-level operators involving  $N\Delta$  intermediate states Eq. (15) (see Fig. 7 for the corresponding diagrams). The other amplitudes in Eq. (A1) are given by the following formulae:

$$\mathcal{M}^{\text{FSI}}[jls, j'l's'] = C_{NB} \sum_{l'', s''} \int \frac{d^3q}{(2\pi)^3} \frac{\tilde{\mathcal{M}}^{\text{prod}}[jls, j'l''s''](p, q) \mathcal{M}_{NB}[j', l''s'', ls](q, p')}{4m_{1'}m_{2'}[q^2/(2\mu_{1'2'}) - (E' - \delta) - i0]} \quad (\text{A2})$$

$$\mathcal{M}^{\text{ISI}}[jls, j'l's'] = C_{NB} \sum_{l'', s''} \int \frac{d^3q}{(2\pi)^3} \frac{\mathcal{M}_{NB}[j, ls, l''s''](p, q) \tilde{\mathcal{M}}^{\text{prod}}[j'l''s'', j'l's'](q, p')}{4m_1m_2[q^2/(2\mu_{12}) - (E - \delta) - i0]} \quad (\text{A3})$$

$$\begin{aligned} \mathcal{M}^{\text{ISI+FSI}}[jls, j'l's'] &= C_{NB} \sum_{l'', s''} \sum_{l''', s'''} \int \frac{d^3q}{(2\pi)^3} \frac{d^3\ell}{(2\pi)^3} \\ &\times \frac{\mathcal{M}_{NB}[j, ls, l''s''](p, q) \tilde{\mathcal{M}}^{\text{prod}}[j'l''s'', j'l'''s'''](q, \ell) \mathcal{M}_{NB}[j', l'''s''', l's'](\ell, p')}{4m_1m_2[q^2/(2\mu_{12}) - (E - \delta) - i0] \cdot 4m_{1'}m_{2'}[\ell^2/(2\mu_{1'2'}) - (E' - \delta) - i0]}, \quad (\text{A4}) \end{aligned}$$

where  $m_{1,2}$  ( $m_{1',2'}$ ) are the masses of the particles in the intermediate state that are related via the  $NN$  interaction to the initial (final) state,  $\mu_{12}$  ( $\mu_{1'2'}$ ) are the corresponding reduced masses,  $E$  ( $E'$ ) is the energy of the initial (final) two-nucleon state in its center-of-mass frame,  $\mathcal{M}_{NB}[j, l_i s_i, l_f s_f]$  is the nucleon-baryon  $NN - NB$  or vice versa half-off shell  $\mathcal{M}$ -matrix (with  $B$  standing for  $N$  or  $\Delta$ ) corresponding to a transition from the state  $(jl_i s_i)$  to the state  $(jl_f s_f)$ , and the sums are over all the intermediate states with given  $j, j'$ ,

<sup>4</sup> In order to unambiguously specify the partial wave, the pion angular momentum should, in general, also be given. We, however, omit it since it is only the  $s$ -wave pion production that is considered here.

$l$ ,  $l'$ ,  $s$ , and  $s'$ . We use the following relation between the  $\mathcal{M}$ -matrix and the commonly used  $\mathcal{T}$ -matrix:  $\mathcal{M}_{NB} = -8\pi^2 \sqrt{m_1 m_2 m_{1'} m_{2'}} \mathcal{T}$ , where the  $m_i$  are the masses of interacting particles. Furthermore, in the formulae given above the coefficient  $C_{NB}$  equals to 1 for NN intermediate states and  $2/\sqrt{2}$  in the case when one of the intermediate states (either initial or final) contains  $\Delta$ <sup>5</sup>. In addition, one has to put  $\delta$  in the propagators to zero ( $\delta = 0$ ) for NN intermediate states while for a  $N\Delta$  intermediate state  $\delta = m_\Delta - m_N$ .

In case of a deuteron in the final state, the corresponding  $\mathcal{M}$  matrices should be replaced by the deuteron wave functions according to

$$\mathcal{M}^{\text{FSI}}[jls, 1] = \frac{1}{\sqrt{2M_N}} \sum_{l''} \int \frac{d^3q}{(2\pi)^3} \tilde{\mathcal{M}}^{\text{prod}}[jls, 1l''s''](p, q) i^{l''} \psi^{l''}(q), \quad (\text{A5})$$

where  $\psi^{l''}(q)$  are the deuteron wave functions corresponding to the angular momentum  $l''$ , normalized by the condition

$$\int \frac{d^3q}{(2\pi)^3} ((\psi^0(q))^2 + (\psi^2(q))^2) = 1. \quad (\text{A6})$$

Thus, the two-nucleon propagator for the deuteron in the final state is absorbed in the wave functions and the normalization has changed. Analogous expressions can be written down for the deuteron in the initial state. Note that in the case of the deuteron in the initial or final state the N<sup>2</sup>LO production operator derived in this paper appears only as the building block for the calculation of the  $\mathcal{M}^{\text{FSI}}$ ,  $\mathcal{M}^{\text{ISI}}$  and  $\mathcal{M}^{\text{ISI+FSI}}$  amplitudes according to Eqs. (A2)–(A4) and (A5), respectively. They do not contribute independently because then there are no free nucleons in the initial or final state.

## Appendix B: The pion-nucleon Lagrangian

The leading order pion nucleon Lagrangian has form

$$\mathcal{L}_{\pi N}^{(1)} = \bar{N} (i v \cdot D + g_A S \cdot u) N. \quad (\text{B1})$$

The pion fields is contained non-linearly in the  $u$ -field which in the sigma gauge is:

$$u(\boldsymbol{\pi}) = \sqrt{U(\boldsymbol{\pi})} = 1 + i \frac{\boldsymbol{\tau} \cdot \boldsymbol{\pi}}{2f_\pi} - \frac{\boldsymbol{\pi}^2}{8f_\pi^2} + i \frac{(\boldsymbol{\tau} \cdot \boldsymbol{\pi})^3}{16f_\pi^3} + \dots \quad (\text{B2})$$

Furthermore, the chiral Lagrangian contains the derivative of the  $u$ -field and the chiral covariant derivative  $D_\mu$  defined as:

$$u_\mu = i (\partial_\mu u u^\dagger + u^\dagger \partial_\mu u), \quad (\text{B3})$$

$$D_\mu = \partial_\mu + \Gamma_\mu, \quad (\text{B4})$$

$$\Gamma_\mu = \frac{1}{2} [u^\dagger, \partial_\mu u]. \quad (\text{B5})$$

<sup>5</sup> Note that keeping  $\Delta$  both in the initial and final states constitutes a higher order effect, as discussed in Sec.III B.

The heavy baryon formalism involves the covariant spin-operator  $S_\mu$  and the four-velocity  $v^\mu$  where

$$S_\mu = \frac{i}{2} \gamma_5 \sigma_{\mu\nu} v^\nu, \quad S \cdot v = 0, \quad \{S_\mu, S_\nu\} = \frac{1}{2} (v_\mu v_\nu - g_{\mu\nu}). \quad (\text{B6})$$

In four-dimensional space-time, the commutator of two spin-operators can be simplified to  $[S_\mu, S_\nu] = i \epsilon_{\mu\nu\gamma\delta} v^\gamma S^\delta$ , where we use the convention  $\epsilon^{0123} = -1$ .

The next order Lagrangian has two derivatives or one  $m_\pi^2$  insertion:

$$\begin{aligned} \mathcal{L}_{\pi N}^{(2)} = \bar{N} \left\{ \frac{1}{2m_N} (v \cdot D)^2 - \frac{1}{2m_N} D \cdot D - \frac{i g_A}{2m_N} \{S \cdot D, v \cdot u\} + c_1 \langle \chi_+ \rangle \right. \\ \left. + \left( c_2 - \frac{g_A^2}{8m_N} \right) (v \cdot u)^2 + c_3 u \cdot u + \left( c_4 + \frac{1}{4m_N} \right) [S^\mu, S^\nu] u_\mu u_\nu \right\} N + \dots, \quad (\text{B7}) \end{aligned}$$

where  $\chi_+ = u^\dagger \chi u^\dagger + u \chi^\dagger u$  ( $\chi = m_\pi^2$  up to isospin violating corrections) and where we have only written those terms relevant for this paper, in addition ' $\langle \dots \rangle$ ' denotes the trace in flavor space.

The relevant third order Lagrangian takes the form

$$\mathcal{L}_{\pi N}^{(3)} = \bar{N} \mathcal{O}_{\text{fixed}}^{(3)} N, \quad (\text{B8})$$

where

$$\begin{aligned} \mathcal{O}_{\text{fixed}}^{(3)} = & \frac{g_A}{8m_N^2} [D^\mu, [D_\mu, S \cdot u]] - i \frac{1}{4m_N^2} (v \cdot D)^3 \\ & - \frac{g_A}{4m_N^2} v \cdot \overleftarrow{D} S \cdot u v \cdot D + \frac{1}{8m_N^2} (i D^2 v \cdot D + \text{h.c.}) \\ & - \frac{g_A}{4m_N^2} (\{S \cdot D, v \cdot u\} v \cdot D + \text{h.c.}) + \frac{3g_A^2}{64m_N^2} (i \langle (v \cdot u)^2 \rangle v \cdot D + \text{h.c.}) \\ & + \frac{1}{32m_N^2} (\epsilon^{\mu\nu\alpha\beta} v_\alpha S_\beta [u_\mu, u_\nu] v \cdot D + \text{h.c.}) \\ & - \frac{g_A}{8m_N^2} (S \cdot u D^2 + \text{h.c.}) - \frac{g_A}{4m_N^2} (S \cdot \overleftarrow{D} u \cdot D + \text{h.c.}) \\ & + \frac{1 + g_A^2 + 8m_N c_4}{16m_N^2} (\epsilon^{\mu\nu\alpha\beta} v_\alpha S_\beta [u_\mu, v \cdot u] D_\nu + \text{h.c.}) \\ & - \frac{g_A^2}{16m_N^2} (i v \cdot u u \cdot D + \text{h.c.}) \\ & + i \frac{1 + 8m_N c_4}{32m_N^2} [v \cdot u, [D^\mu, u_\mu]] + \frac{c_2}{2m_N} (i \langle v \cdot u u_\mu \rangle D^\mu + \text{h.c.}) + \dots \quad (\text{B9}) \end{aligned}$$

## Appendix C: Basic integrals

### 1. Definitions and analytic expressions for various integrals

In this subsection we give the explicit definitions of the common dimensionless loop integrals used in this work. The first integral  $J_{\pi\Delta} = \mu^\epsilon J_0(-\delta)$  where  $\mu$  is the dimension-

regularization scale and the integral  $J_0(-\delta)$  is defined in Ref. [36].

$$\begin{aligned} \frac{1}{\delta} J_{\pi\Delta}(\delta) &= \frac{\mu^\epsilon}{i\delta} \int \frac{d^{4-\epsilon}l}{(2\pi)^{4-\epsilon}} \frac{1}{(l^2 - m_\pi^2 + i0)(-v \cdot l - \delta + i0)} \\ &= 4L + \frac{(-2)}{(4\pi)^2} \left[ -1 + \log\left(\frac{\mu^2}{m_\pi^2}\right) \right] \\ &\quad + \frac{4}{(4\pi)^2} \left[ -1 + \frac{\sqrt{1-y-i0}}{\sqrt{y}} \left[ -\frac{\pi}{2} + \arctan\left(\frac{\sqrt{y}}{\sqrt{1-y-i0}}\right) \right] \right], \end{aligned} \quad (\text{C1})$$

$$\begin{aligned} I_{\pi\pi}(k_1^2) &= \frac{\mu^\epsilon}{i} \int \frac{d^{4-\epsilon}l}{(2\pi)^{4-\epsilon}} \frac{1}{(l^2 - m_\pi^2 + i0)((l+k_1)^2 - m_\pi^2 + i0)} \\ &= -2L - \frac{1}{(4\pi)^2} \left[ \log\left(\frac{m_\pi^2}{\mu^2}\right) - 1 + 2F_1\left(\frac{k_1^2}{m_\pi^2}\right) \right], \end{aligned} \quad (\text{C2})$$

where

$$F_1(x) = \frac{\sqrt{4-x-i0}}{\sqrt{x}} \arctan\left(\frac{\sqrt{x}}{\sqrt{4-x-i0}}\right), \quad (\text{C3})$$

$$L = \frac{1}{(4\pi)^2} \left[ -\frac{1}{\epsilon} + \frac{1}{2}(\gamma_E - 1 - \log(4\pi)) \right], \quad (\text{C4})$$

and the variables  $x, y$  are defined via  $x = k_1^2/m_\pi^2, y = \delta^2/m_\pi^2$ .

Further, the integrals in Eqs. (C5) and (C6) can be reduced to simple one-dimensional integrals which can be calculated numerically.

$$\delta J_{\pi\pi\Delta} = \delta \frac{\mu^\epsilon}{i} \int \frac{d^{4-\epsilon}l}{(2\pi)^{4-\epsilon}} \frac{1}{(l^2 - m_\pi^2 + i0)((l+k_1)^2 - m_\pi^2 + i0)(-v \cdot l - \delta + i0)}, \quad (\text{C5})$$

$$\begin{aligned} k_1^2 J_{\pi\pi N\Delta} &= k_1^2 \frac{\mu^\epsilon}{i} \int \frac{d^{4-\epsilon}l}{(2\pi)^{4-\epsilon}} \left[ \frac{1}{(l^2 - m_\pi^2 + i0)((l+k_1)^2 - m_\pi^2 + i0)} \right. \\ &\quad \left. \times \frac{1}{(-v \cdot l + i0)(-v \cdot l - \delta + i0)} \right]. \end{aligned} \quad (\text{C6})$$

It is also convenient to define finite, scale-independent parts of  $J_{\pi\Delta}$  and  $I_{\pi\pi}$  in which the divergency  $L$  and the  $\log(m_\pi/\mu)$  terms are removed. The finite contributions  $J_{\pi\Delta}^{\text{finite}}$  and  $I_{\pi\pi}^{\text{finite}}$  will be used in the subsequent section.

$$I_{\pi\pi} = -2L - \frac{1}{(4\pi)^2} \log\left(\frac{m_\pi^2}{\mu^2}\right) + I_{\pi\pi}^{\text{finite}}, \quad (\text{C7})$$

$$I_{\pi\pi}^{\text{finite}} = \frac{1}{(4\pi)^2} \left( 1 - 2 \frac{\sqrt{4-x-i0}}{\sqrt{x}} \arctan\left(\frac{\sqrt{x}}{\sqrt{4-x-i0}}\right) \right), \quad (\text{C8})$$

$$\frac{1}{\delta} J_{\pi\Delta} = 4L + \frac{2}{(4\pi)^2} \log\left(\frac{m_\pi^2}{\mu^2}\right) + \frac{1}{\delta} J_{\pi\Delta}^{\text{finite}}, \quad (\text{C9})$$

$$\frac{1}{\delta} J_{\pi\Delta}^{\text{finite}} = \frac{4}{(4\pi)^2} \left[ -\frac{1}{2} + \frac{\sqrt{1-y-i0}}{\sqrt{y}} \left[ -\frac{\pi}{2} + \arctan\left(\frac{\sqrt{y}}{\sqrt{1-y-i0}}\right) \right] \right]. \quad (\text{C10})$$

From the expressions above it is easy to obtain the important relation, which is used in the analysis of the integral combinations, relevant for our study

$$I_{\pi\pi} + \frac{1}{2\delta} J_{\pi\Delta} = I_{\pi\pi}^{\text{finite}} + \frac{1}{2\delta} J_{\pi\Delta}^{\text{finite}}. \quad (\text{C11})$$

## 2. Combinations of basic integrals in the limit $\delta \rightarrow \infty$

In this subsection we discuss the behavior of the integral combinations, see Eqs. (20)–(22), relevant for loop-diagrams considered in this work. While the integrals  $I_{\pi\pi}$  and  $J_{\pi\Delta}$  have analytic expressions for any  $\delta$ , the integral  $J_{\pi\pi\Delta}$  can be done analytically only in the limit  $\delta \rightarrow \infty$ . Using the dispersive analysis, one finds the asymptotic expression for  $\delta J_{\pi\pi\Delta}$  when  $\delta \rightarrow \infty$

$$(4\pi)^2 \delta J_{\pi\pi\Delta} = 2 \log \left[ \frac{m_\pi}{2\delta} \right] - 1 - (4\pi)^2 I_{\pi\pi}^{\text{finite}} + \frac{1}{36\delta^2} \left( (36m_\pi^2 - 6k_1^2) \log \left[ \frac{m_\pi}{2\delta} \right] - k_1^2 + 6m_\pi^2 + (3k_1^2 - 12m_\pi^2)(4\pi)^2 I_{\pi\pi}^{\text{finite}} \right) + O\left(\frac{1}{\delta^3}\right). \quad (\text{C12})$$

Note that to get the MCS terms relevant at N<sup>2</sup>LO, one ignores  $m_\pi^2$  compared to  $k_1^2$  in the last two lines of the expression above.

Using the expression above, Eq. (C11) and the expansion of  $J_{\pi\Delta}^{\text{finite}}$  for large  $\delta$

$$\frac{(4\pi)^2}{\delta} J_{\pi\Delta}^{\text{finite}} = -4 \log \left[ \frac{m_\pi}{2\delta} \right] - 2 + \frac{m_\pi^2}{\delta^2} \left( 2 \log \left[ \frac{m_\pi}{2\delta} \right] - 1 \right) + O\left(\frac{1}{\delta^4}\right), \quad (\text{C13})$$

one obtains

$$\left( I_{\pi\pi} + \delta J_{\pi\pi\Delta} + \frac{1}{2} \frac{J_{\pi\Delta}}{\delta} + \frac{2}{(4\pi)^2} \right) = O\left(\frac{1}{\delta^2}\right). \quad (\text{C14})$$

Thus, this combination vanishes in the limit  $\delta \rightarrow \infty$ .

Analogously, one finds

$$\begin{aligned} & \frac{\delta^2}{k_1^2} \left( I_{\pi\pi} + \delta J_{\pi\pi\Delta} + \frac{1}{2} \frac{J_{\pi\Delta}}{\delta} + \frac{2}{(4\pi)^2} \right) - \frac{1}{12} \left( I_{\pi\pi} + \frac{1}{2} \frac{J_{\pi\Delta}}{\delta} + \frac{1}{3} \frac{2}{(4\pi)^2} \right) \\ &= \frac{m_\pi^2}{3k_1^2} \left( 6 \log \left[ \frac{m_\pi}{2\delta} \right] - 1 - I_{\pi\pi}^{\text{finite}} \right) + O\left(\frac{1}{\delta^2}\right). \end{aligned} \quad (\text{C15})$$

This combination vanishes in the limit  $\delta \rightarrow \infty$  up to higher order terms. To make it vanishing also at higher order one would need to extend the calculation and keep the so far neglected higher order terms.

Finally, the integral  $J_{\pi\pi N\Delta}$  obviously vanishes at large  $\delta$

$$J_{\pi\pi N\Delta} = \frac{1}{\delta} (J_{\pi\pi\Delta} - J_{\pi\pi N}), \quad (\text{C16})$$

where  $J_{\pi\pi N} = J_{\pi\pi\Delta}(\delta = 0)$ .

- 
- [1] T. D. Cohen, J. L. Friar, G. A. Miller and U. van Kolck, Phys. Rev. C **53**, 2661 (1996).
  - [2] B. Y. Park, F. Myhrer, J. R. Morones, T. Meissner and K. Kubodera, Phys. Rev. C **53**, 1519 (1996).
  - [3] C. Hanhart, Phys. Rept. **397**, 155 (2004).

- [4] V. Baru, C. Hanhart, and F. Myhrer, “Effective field theory calculations for  $NN \rightarrow NN\pi$ ”, in preparation
- [5] V. Bernard, Prog. Part. Nucl. Phys. **60**, 82 (2008).
- [6] E. Epelbaum, H.-W. Hammer and U.-G. Meißner, Rev. Mod. Phys. **81**, 1773 (2009).
- [7] T. Sato, T. S. H. Lee, F. Myhrer and K. Kubodera, Phys. Rev. C **56**, 1246 (1997).
- [8] C. Hanhart, J. Haidenbauer, M. Hoffmann, U.-G. Meißner and J. Speth, Phys. Lett. B **424**, 8 (1998).
- [9] V. Dmitrasinovic, K. Kubodera, F. Myhrer and T. Sato, Phys. Lett. B **465**, 43 (1999).
- [10] S. Ando, T.-S. Park and D.-P. Min, Phys. Lett. B **509**, 253 (2001).
- [11] V. Bernard, N. Kaiser and U.-G. Meißner, Eur. Phys. J. A **4**, 259 (1999).
- [12] C. A. da Rocha, G. A. Miller and U. van Kolck, Phys. Rev. C **61**, 034613 (2000).
- [13] C. Hanhart and N. Kaiser, Phys. Rev. C **66**, 054005 (2002) .
- [14] V. Lensky, V. Baru, J. Haidenbauer, C. Hanhart, A. E. Kudryavtsev and U.-G. Meißner, Eur. Phys. J. A **27**, 37 (2006).
- [15] Y. Kim, T. Sato, F. Myhrer and K. Kubodera, Phys. Rev. C **80**, 015206 (2009).
- [16] A. A. Filin, V. Baru, E. Epelbaum, H. Krebs, C. Hanhart, A. E. Kudryavtsev and F. Myhrer, Phys. Rev. C **85**, 054001 (2012).
- [17] C. Hanhart and A. Wirzba, Phys. Lett. B **650**, 354 (2007).
- [18] D. R. Bolton and G. A. Miller, Phys. Rev. C **83**, 064003 (2011).
- [19] C. Hanhart, U. van Kolck and G. A. Miller, Phys. Rev. Lett. **85**, 2905 (2000).
- [20] V. Baru, E. Epelbaum, J. Haidenbauer, C. Hanhart, A. E. Kudryavtsev, V. Lensky and U.-G. Meißner, Phys. Rev. C **80**, 044003 (2009).
- [21] S. X. Nakamura, Phys. Rev. C **77**, 054001 (2008).
- [22] U. van Kolck, J. A. Niskanen and G. A. Miller, Phys. Lett. B **493**, 65 (2000).
- [23] A.A. Filin, V. Baru, E. Epelbaum, J. Haidenbauer, C. Hanhart, A. E. Kudryavtsev and U.-G. Meißner, Phys. Lett. B **681**, 423 (2009).
- [24] D. R. Bolton and G. A. Miller, Phys. Rev. C **81**, 014001 (2010).
- [25] D. S. Koltun and A. Reitan, Phys. Rev. **141**, 1413 (1966).
- [26] T. S. H. Lee and D. O. Riska, Phys. Rev. Lett. **70**, 2237 (1993).
- [27] C. J. Horowitz, H. O. Meyer and D. K. Griegel, Phys. Rev. C **49**, 1337 (1994).
- [28] C. J. Horowitz, Phys. Rev. C **48**, 2920 (1993).
- [29] J. A. Niskanen, Phys. Rev. C **53**, 526, (1996).
- [30] E. Hernandez and E. Oset, Phys. Lett. B **350**, 158 (1995).
- [31] C. Hanhart, J. Haidenbauer, A. Reuber, C. Schutz and J. Speth, Phys. Lett. B **358**, 21 (1995).
- [32] C. Hanhart, J. Haidenbauer, O. Krehl and J. Speth, Phys. Lett. B **444**, 25 (1998).
- [33] V. Pascalutsa and D. R. Phillips, Phys. Rev. C **67**, 055202 (2003).
- [34] V. Baru, J. Haidenbauer, C. Hanhart, A. E. Kudryavtsev, V. Lensky and U.-G. Meißner, in *Proceedings of 11-th International Conference on Meson-Nucleon Physics and the Structure of the Nucleon (MENU 2007), Jülich, Germany*, eConfC **070910** 128 (2007); [arXiv:0711.2748 [nucl-th]].
- [35] C. Ordóñez, L. Ray and U. van Kolck, Phys. Rev. C **53**, 2086 (1996).
- [36] V. Bernard, N. Kaiser and U.-G. Meißner, Int. J. Mod. Phys. E **4**, 193 (1995).
- [37] N. Fettes, U.-G. Meißner and S. Steininger, Nucl. Phys. A **640**, 199 (1998); N. Fettes, Ph.D. thesis, Bonn University, 2000.
- [38] N. Fettes, U.-G. Meißner, M. Mojzis and S. Steininger, Annals Phys. **283**, 273 (2000) [Erratum-ibid. **288**, 249 (2001)].

- [39] A. Gårdestig, D. R. Phillips and C. Elster, *Phys. Rev. C* **73**, 024002 (2006).
- [40] T. R. Hemmert, PhD-thesis, University of Massachusetts Amherst (1999).
- [41] T. R. Hemmert, B. R. Holstein and J. Kambor, *J. Phys. G* **24**, 1831 (1998).
- [42] N. Fettes and U. G. Meißner, *Nucl. Phys. A* **679**, 629 (2001).
- [43] N. Kaiser, S. Gerstendorfer, W. Weise, *Nucl. Phys. A* **637**, 395 (1998).
- [44] S. Weinberg, *Phys. Lett. B* **251**, 288 (1990).
- [45] S. Weinberg, *Nucl. Phys. B* **363**, 3 (1991).
- [46] J. Haidenbauer, K. Holinde and M. B. Johnson, *Phys. Rev. C* **48**, 2190 (1993).
- [47] R. Machleidt, *Phys. Rev. C* **63**, 024001 (2001).
- [48] V. Bernard, H. W. Fearing, T. R. Hemmert and U.-G. Meißner, *Nucl. Phys. A* **635**, 121 (1998)  
[Erratum-ibid. A **642**, 563 (1998)] [*Nucl. Phys. A* **642**, 563 (1998)].
- [49] T. Appelquist and J. Carazzone, *Phys. Rev. D* **11**, 2856 (1975); Lowell S. Brown, *Phys. Rev. D* **39**, 3084 (1989).
- [50] M. Cleven, F.-K. Guo, C. Hanhart and U.-G. Meißner, *Eur. Phys. J. A* **47**, 120 (2011).